ANALYSIS AND DESIGN OF HIGHLY TRANSPARENT AND EFFICIENT ANTENNA

A THESIS SUBMITTED TO
THE GRADUATE SCHOOL OF NATURAL AND APPLIED SCIENCES
OF
MIDDLE EAST TECHNICAL UNIVERSITY

BY

MEHMET EMRE ERALP

IN PARTIAL FULFILLMENT OF THE REQUIREMENTS
FOR
THE DEGREE OF MASTER OF SCIENCE
IN
ELECTRICAL AND ELECTRONICS ENGINEERING

JANUARY 2025

Approval of the thesis:

ANALYSIS AND DESIGN OF HIGHLY TRANSPARENT AND EFFICIENT ANTENNA

submitted by **MEHMET EMRE ERALP** in partial fulfillment of the requirements for the degree of **Master of Science in Electrical and Electronics Engineering Department, Middle East Technical University** by,

Prof. Dr. Naci Emre Altun
Dean, Graduate School of **Natural and Applied Sciences** _____

Prof. Dr. İlkay Ulusoy
Head of Department, **Electrical and Electronics Engineering** _____

Prof. Dr. Özlem Aydın Çivi
Supervisor, **Electrical and Electronics Engineering, METU** _____

Assoc. Prof. Dr. Reyhan Baktur
Co-supervisor, **Electrical and Computer Eng., USU, UT, USA** _____

Examining Committee Members:

Prof. Dr. Sencer Koç
Electrical and Electronics Engineering, METU _____

Prof. Dr. Özlem Aydın Çivi
Electrical and Electronics Engineering, METU _____

Prof. Dr. Gülbin Dural
Electrical and Electronics Engineering, METU _____

Assoc. Prof. Dr. Lale Alatan
Electrical and Electronics Engineering, METU _____

Prof. Dr. Vakur B. Ertürk
Electrical and Electronics Engineering, Bilkent University _____

Date: 08.01.2025

I hereby declare that all information in this document has been obtained and presented in accordance with academic rules and ethical conduct. I also declare that, as required by these rules and conduct, I have fully cited and referenced all material and results that are not original to this work.

Name, Surname: Mehmet Emre Eralp

Signature :

ABSTRACT

ANALYSIS AND DESIGN OF HIGHLY TRANSPARENT AND EFFICIENT ANTENNA

Eralp, Mehmet Emre
M.S., Department of Electrical and Electronics Engineering
Supervisor: Prof. Dr. Özlem Aydın Çivi
Co-Supervisor: Assoc. Prof. Dr. Reyhan Baktur

January 2025, 64 pages

This thesis investigates the analysis, design, and fabrication of optically transparent antennas, addressing the trade-offs between transparency and radiation efficiency. Transparent monopole and patch antennas are explored, focusing on their potential applications in beyond 5G and vehicle-to-everything (V2X) communication systems. The transparent planar monopole antenna features a single-sided geometry on flexible PET substrates coated with silver nanowires (AgNW). The fundamental factors limiting the efficiency of the monopole are analyzed, and effective antenna topologies and methods to enhance efficiency are presented. The study demonstrates that widening the monopole geometry and strategically adding highly conductive strips can significantly improve radiation efficiency without substantially compromising transparency. Fabricated prototypes operate over a wide frequency range, covering 3.5 GHz and 5.9 GHz, achieving efficiencies of 50.4% and 76.3%, respectively, with optical transparency reaching 80%. Additionally, the primary factors limiting the gain of optically transparent patch antennas are analyzed, and strategies for gain enhancement are outlined. The research introduces a circuit model predicting further improvements and

proposes an efficient patch antenna design. The patch antenna is fabricated using AgNWs with low-cost manufacturing methods and validated through measurements. The proposed patch antenna achieves a gain of 3.58 dBi and an efficiency of 44% at 8.9 GHz.

Keywords: Transparent Antenna, Silver Nanowires, Optical Transparency, Surface Resistance, Optically Transparent Conductors.

ÖZ

YÜKSEK ŞEFFAF VE VERİMLİ ANTENLERİN ANALİZİ VE TASARIMI

Eralp, Mehmet Emre
Yüksek Lisans, Elektrik ve Elektronik Mühendisliği Bölümü
Tez Yöneticisi: Prof. Dr. Özlem Aydın Çivi
Ortak Tez Yöneticisi: Doç. Dr. Reyhan Baktur

Ocak 2025 , 64 sayfa

Optik olarak şeffaf antenlerin analizi, tasarımı ve üretimi üzerine çalışılmış ve şeffaflık ile radyasyon verimliliği arasındaki denge ele alınmıştır. Şeffaf tekkutup ve yama antenler, 5G sonrası ve araçtan her şeye (V2X) haberleşme sistemlerindeki potansiyel uygulamalarına odaklanılarak incelenmiştir. Şeffaf düzlemsel tekkutup anten, gümüş nanotel (AgNW) ile kaplanmış esnek PET alt tabakalar üzerinde tek taraflı bir geometrik yapıya sahiptir. Tekkutup antenin verimliliğini sınırlayan temel faktörler analiz edilmiş ve verimliliği artırmak için etkili anten topolojileri ve yöntemleri sunulmuştur. Çalışma, tekkutup geometrisini genişletmenin ve stratejik olarak yüksek iletkenliğe sahip şeritler eklemenin, şeffaflıktan büyük ölçüde ödün vermeden radyasyon verimliliğini önemli ölçüde artırabileceğini göstermektedir. Üretilen prototipler, 3.5 GHz ve 5.9 GHz bantlarını kapsayan geniş bir frekans aralığında çalışarak sırasıyla %50.4 ve %76.3 verimlilik değerlerine ve %80 optik şeffaflığa ulaşmıştır. Ayrıca, optik olarak şeffaf yama antenlerin kazancını sınırlayan birincil faktörler analiz edilmiş ve kazanç artırımı için stratejiler sunulmuştur. Araştırma, kazançta daha fazla iyileştirme öngören bir devre modeli tanıtmakta ve verimli bir yama anten tasarımı

önermektedir. Yama anten, düşük maliyetli üretim yöntemleri kullanılarak AgNW ile üretilmiş ve ölçümlerle doğrulanmıştır. Önerilen yama anten, 8.9 GHz'de 3.58 dBi kazanç ve %44 verimlilik değerine ulaşmıştır.

Anahtar Kelimeler: Şeffaf Anten, Gümüş Nanotel, Optik Şeffaflık, Yüzey Direnci, Optik Şeffaf İletkenler.

To a better world.

ACKNOWLEDGMENTS

I would like to express my deepest gratitude to my supervisor, Prof. Özlem Aydın Çivi, for her invaluable guidance, unwavering support, and exceptional expertise throughout my thesis work. Her insightful advice and encouragement have been a constant source of inspiration.

I am also profoundly thankful to my co-supervisor, Assoc. Prof. Reyhan Baktur, whose dedication and commitment to this research were nothing short of extraordinary. Her meticulous attention to detail, determination, and passion for the work inspired me at every stage of the research.

I am grateful to the thesis jury members, Prof. Sencer Koç, Prof. Gülbin Dural, Assoc. Prof. Lale Alatan, and Prof. Vakur Ertürk, for their comments and contributions.

In addition, I am deeply grateful to Accelerate Simulation Technologies, and its co-founders, Uğur Oğuz and Prof. Özgür Ergül, for their full support. Their encouragement and belief in my potential have been invaluable.

I would like to extend my heartfelt thanks to Onuralp Çakır and Prof. Emrah Ünalan for their support. Their expertise and assistance were critical to the experimental aspects of this work, and their contributions are deeply appreciated.

I wish to express my sincere appreciation to my colleagues, Özgür Eriş and Ali Samet Ayık, for their collaboration, insights, and support during this work.

I also wish to gratefully acknowledge the financial support provided by the TÜBİTAK 2210-A Scholarship Program during my Master's thesis.

Finally, I would like to extend my deepest thanks to my family, my beloved friends, and my best friend for their encouragement and support. Their belief in me and their presence in my life have been my greatest sources of strength and motivation.

TABLE OF CONTENTS

LIST OF TABLES

TABLES

LIST OF FIGURES

FIGURES

LIST OF ABBREVIATIONS

V2X	Vehicle-To-Everything
MIMO	Multiple Input Multiple Output
5G	Fifth Generation
PEC	Perfect Electric Conductor
TCO	Transparent Conductive Oxide
ITO	Indium Tin Oxide
IZTO	Indium Zinc Tin Oxide
AZO	Aluminum-doped Zinc Oxide
GZO	Gallium-doped Zinc Oxide
AgNW	Silver Nanowires
CuNW	Copper Nanowires
PET	Polyethylene Terephthalate
TPU	Thermoplastic Polyurethane
CPW	Coplanar Waveguide

CHAPTER 1

INTRODUCTION

In today's hyper-connected world, the demand for seamless communication and efficient data transmission is more critical than ever. The concepts of multi-point connectivity, low latency, and massive device connections are at the forefront of this technological evolution. Optically transparent antennas represent an emerging and versatile technology with applications in various domains such as vehicle-to-everything (V2X) communication, smart buildings, urban networks, and medical systems. Their ability to seamlessly integrate into glass surfaces, such as vehicle windshields, architectural glass, and displays, makes them highly desirable for modern, unobtrusive wireless communication solutions. These antennas enable V2X systems to facilitate communication between vehicles, infrastructure, and even satellites without compromising visual aesthetics or clarity. They hold potential for deployment on solar panels in CubeSats and in indoor relay networks for future technologies like 6G [2], [3].

The transparency of antennas is typically achieved through two main approaches: meshed conductors or transparent conductive film materials. While meshed conductors are relatively straightforward and effective, they remain visually perceptible. On the other hand, transparent conductive materials, such as indium tin oxide (ITO), indium zinc tin oxide (IZTO), and silver nanowires (AgNW), offer a better balance between optical transparency and electrical conductivity. However, these materials often face challenges in optimizing antenna efficiency, design complexity, and fabrication methods. Transparent patch antennas, in particular, encounter significant efficiency losses when both the radiator and ground plane are made transparent. Besides, majority of the prior transparent conductive film antenna designs have less than 50% radiation efficiency [2].

Meshed-type transparent antennas have been a subject of research since their early studies in 2004 [4], with significant advancements made in recent years. A high-gain optically transparent grid array antenna for millimeter-wave frequencies has been introduced [5], while a slot loop antenna utilizing a metal-mesh-based transparent film for wearable glasses operating at 2.4 GHz has been developed [6]. A patch antenna with filtering capabilities for sub-6 GHz 5G applications has been proposed [7], and antennas embedded in active display panels, such as OLEDs and LCDs, for millimeter-wave 5G devices have been investigated [8]. Refined meshed patch antennas integrated with solar panels have also been explored, highlighting their potential in energy-sustainable systems [9]. An optically transparent right-handed circularly polarized reflectarray featuring fine metal line meshes for Ka-band satellite communication has been proposed [10], and a meshed transparent transmitarray operating at 28 GHz for 5G systems has been designed [11]. Additionally, a flexible and robust passive UHF circularly polarized tag antenna using a mesh conductor polymer has been demonstrated [12]. These studies present the versatility of meshed-type transparent antennas with their applications across wearable devices, smart displays, high-frequency communication systems, and energy-integrated platforms, while addressing challenges related to transparency and efficiency.

Transparent conductive film antennas have attracted considerable attention due to their potential for combining functionality with optical clarity. ITO has been extensively utilized, with designs such as an optically transparent MIMO antenna for automotive applications [13] and a similar MIMO antenna for 5G smartphones operating in the microwave and millimeter-wave bands [14]. Significant progress has also been made in wearable device applications, including a study on glasses-based antennas using IZTO, achieving an efficiency of 46% [15]. Reflectarray antennas made from ITO have been proposed for various applications, including integration into windows, transparent media, and electronic casings, offering aesthetic and security benefits [16]. Material-focused studies have introduced highly transparent ultra-wideband antennas constructed from multilayered ITO/Ag/ITO electrode films [17]. Gallium-doped zinc oxide (GZO) has also been explored, with antenna arrays exhibiting high transparency, intended for 5G networks in smart cities [18]. Beyond transparent oxides, silver nanowire (AgNW) antennas have demonstrated promise, including

screen-printed bowtie antennas with efficiencies around 50% [19], and patch antennas achieving transparency levels of 51% at 24 GHz and 61 GHz, though with simulated efficiencies of 8.9% and 49.4%, respectively [20]. These studies collectively highlight the advancements in transparent conductive film antennas, emphasizing their applicability across automotive, wearable, and urban communication technologies, while addressing the ongoing challenges of efficiency and fabrication. Notably, the above-mentioned works often involve more complex fabrication cycles, such as clean room operations, sputtering, photolithography, and screen printing. In contrast, a simpler and lower-cost method—air spraying AgNW—has been utilized in this thesis work for antenna fabrication. Furthermore, when compared to the AgNW bowtie and patch antennas mentioned above, the monopole and patch antennas designed in this work achieved higher measured efficiencies of 76.3% and 44%, respectively.

1.1 Scope of the Thesis and Main Contributions

This thesis research explores the fundamental trade-offs in achieving optically transparent antennas, focusing on efficiency improvement, design simplicity, and cost-effective fabrication. It presents promising solutions for both transparent monopole and transparent patch antennas.

Transparent Monopole Antenna:

- The monopole is designed as a single-sided planar geometry on flexible substrates like polyethylene terephthalate (PET), utilizing a coplanar waveguide (CPW) feed. The design eliminates the need for a ground plane, making it suitable for flush mounting or integration as a sticker on surfaces such as glass.
- The study explores the fundamental factors that limit radiation efficiency and reduce gain in transparent planar monopole antennas. It proposes strategies to mitigate these challenges.
- Gain improvement methods are proposed, such as widening the antenna geometry and strategically placing thin, highly conductive strips where the current is induced densely.

- Simulation methodologies for studying extremely thin conductive films, in the range of tens of nanometers, using both 3D meshing of thin solid geometries and 2D impedance boundary surfaces are stated. These methods provide consistent and accurate results.
- Two monopole prototypes are fabricated using AgNW-coated PET films. The monopole with good conductor strips achieves high radiation efficiency while maintaining good optical transparency.

Transparent Patch Antenna:

- A fully transparent patch antenna is introduced, with both the radiator and ground plane fabricated using a AgNW applied via airbrushing onto PET substrates.
- The research identifies the primary factors contributing to the reduction in radiation efficiency and gain for transparent patch antennas.
- Several strategies are proposed to enhance antenna performance, including the use of thicker substrates and operation at higher frequencies.
- A closely layered structure is introduced to further minimize loss resistance, achieved by coating both sides of the PET films with AgNW to create a double-sided conductive surface.
- Multiple prototypes of the patch antenna are fabricated, successfully achieving a balance between antenna gain and optical transparency.

By addressing the efficiency limitations of transparent antennas and proposing reliable fabrication techniques, this work contributes to advancing the integration of optically transparent antennas across a range of innovative applications.

This thesis is organized into five chapters.

Chapter 2 provides an overview of transparent antenna classifications, focusing on meshed conductors and transparent conductive film materials. The challenges arising from the trade-off between transparency and efficiency are discussed in detail. Surface resistance is introduced as a practical metric to evaluate this trade-off. Materials

such as AgNW and CuNW are briefly described, including their preparation methods and key properties.

Chapter 3 outlines the analyses and design procedures for transparent monopole antennas. It presents the theoretical underpinnings of the designs, simulation results, and fabrication techniques. Moreover, measurement results for the fabricated prototypes are reported and discussed.

Chapter 4 states the analyses of transparent patch antennas. It details the design methodologies, the materials and techniques employed, and the results of experimental measurements. The findings highlight the performance characteristics and trade-offs specific to AgNW transparent patch antennas.

Finally, Chapter 5 concludes the thesis by summarizing the key findings and contributions of the research, providing insights for future work in the field of transparent antenna technologies.

CHAPTER 2

DISCUSSIONS ON OPTICALLY TRANSPARENT ANTENNAS AND TRANSPARENT CONDUCTIVE MATERIALS

2.1 Introduction

Optically transparent antennas are designed to be visually unobtrusive by ensuring that their radiating elements allow light to pass through while maintaining their ability to efficiently transmit and receive electromagnetic waves. Achieving this optical transparency requires careful material selection and design strategies to balance electrical conductivity with visual transparency. As stated in Ch. 1, there are two primary approaches to making antennas optically transparent: employing meshed conductors and using transparent conductive films, as illustrated in Fig. 2.1.

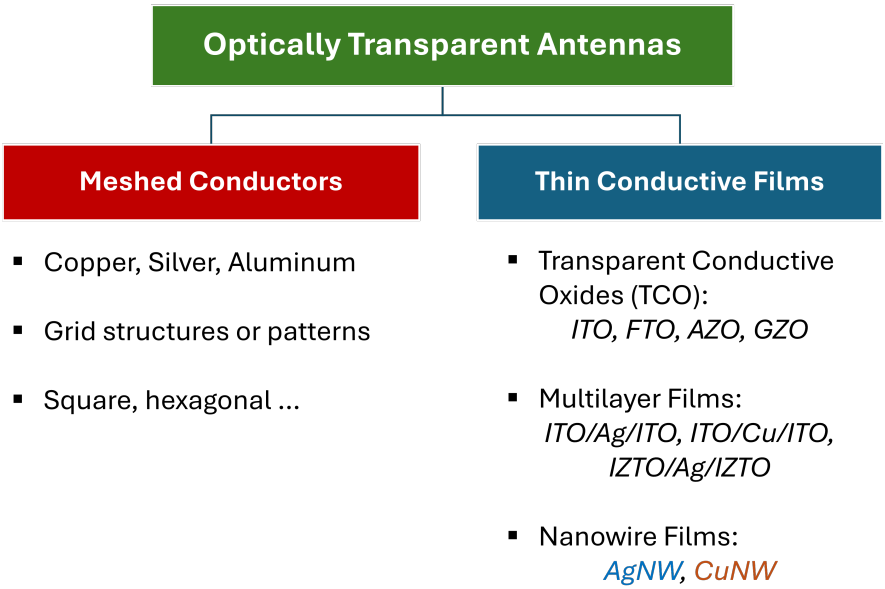

Figure 2.1: Optically transparent antenna classification and materials.

Meshed conductors are thin metallic grids or lattices that cover only a small portion of the antenna's surface as depicted in Fig. 2.2a. By creating openings in the grid structure, a significant amount of light is allowed to pass through, achieving optical transparency. The geometry of the grid, including the width and spacing of the mesh, is optimized to maintain good electrical conductivity while reducing visual obstruction [4], [21]. Copper and silver meshes are commonly used for such grid structures due to their ability to achieve a reasonable balance between transparency and conductivity. However, when these meshes are densely placed or the line width is large enough to enhance conductivity, the antenna becomes visually perceptible as shown in Fig. 2.2b. This visual perceptibility can compromise the aesthetic appeal, particularly in applications that demand near-invisible designs. Although copper meshes are effective in providing good conductivity and transparency, their appearance poses an issue to be considered by a designer in achieving the desired level of clearance.

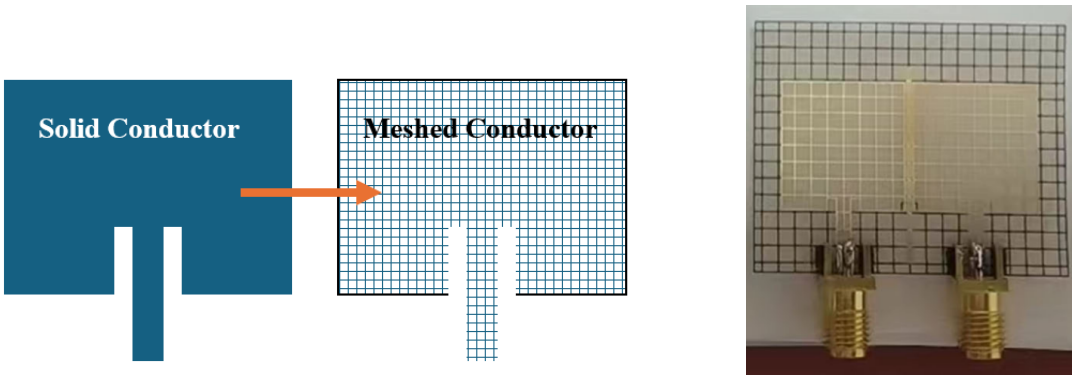

(a) (b)

Figure 2.2: Meshed conductor antennas: (a) a visual for meshed antenna geometry, (b) wired metal mesh MIMO antenna example [1].

Transparent conductive films, on the other hand, are materials that have inherent transparency in the visible spectrum and provide electrical conductivity to support electromagnetic radiation. These materials achieve transparency because of their ability to interact minimally with visible light, either through a high optical band-gap or nanoscale structural properties that allow light to pass through. However, the conductivity they provide is significantly lower than that of traditional antenna conductors such as copper or silver. This reduced conductivity introduces trade-offs in antenna

performance, particularly in terms of radiation efficiency and gain, which must be carefully addressed in the design process. Despite these limitations, their ability to achieve a high degree of transparency makes them a compelling choice for optically transparent antenna designs.

(a) ITO [13] (b) FTO [22] (c) AZO/Ag/AZO

(d) IZTO/Ag/IZTO [15] (e) AgNW (f) CuNW

Figure 2.3: Transparent conductive film examples.

Transparent conductive oxides (TCOs) are the most widely studied optically transparent conductors. These materials are wide-bandgap semiconductors, typically oxide compounds doped with metals. They operate within the physical limitations defined by the plasma frequency, a concept derived from the Drude free-electron model [23]. Unlike metals like copper, which reflect most incident electromagnetic waves due to their plasma frequency in the X-ray region, TCOs have plasma frequencies in the infrared (IR) range, making them transparent to visible light while remaining electrically conductive [24]. Some examples can be seen in Fig. 2.3.

Indium tin oxide (ITO) is the most common TCO, with a large industrial base. It can offer a reasonable conductivity around 10^6 S/m and optical transparency between 75% and 92% at 550 *nm*. It is widely used in transparent antenna designs, whose one

example is shown in [13], due to its mature manufacturing processes and deposition on rigid substrates (e.g., glass or plastic). However, ITO is brittle and poses challenges, such as the toxicity of indium during manufacturing and supply-chain issues due to indium's rarity as a resource. Besides, aluminum-doped zinc oxide (AZO) has emerged as a promising alternative to ITO, providing similar transparency and lower resistance. It is non-toxic and relies on abundant raw materials, making it environmentally friendly and cost-effective. However, its adoption is limited by the lack of large-scale deposition techniques and industrial support compared to ITO. Other TCOs include fluorine-doped tin oxide (FTO) and gallium-doped zinc oxide (GZO), along with various multilayer TCO films. These materials exhibit similar performance to ITO and AZO but lack significant advantages in conductivity, transparency, or scalability. Consequently, they remain underexplored compared to the dominant TCOs [2].

Multilayer films, such as ITO/Ag/ITO, ITO/Cu/ITO, indium–zinc–tin oxide layers (IZTO/Ag/IZTO) and AZO/Ag/AZO, represent a sophisticated approach to balancing transparency and electrical conductivity in optically transparent antennas. These multilayer films combine the transparency of oxides like ITO or AZO with the excellent conductivity of very thin silver or copper films. For example, ITO/Ag/ITO [17] or IZTO/Ag/IZTO [15] films exhibit lower resistance and high transparency, making them a good choice for efficient antennas. Similarly, AZO/Ag/AZO structures provide comparable performance while utilizing non-toxic and abundant materials like AZO, offering an environmentally friendly alternative. However, these multilayer configurations come with notable challenges. Their fabrication is often complex and costly, requiring precise deposition techniques like sputtering or thermal evaporation to ensure uniformity and avoid defects.

Silver nanowires (AgNWs) and copper nanowires (CuNWs) shown in Fig. 2.3e and Fig. 2.3f are emerging materials in a range of electronic applications as transparent conductive films. With their electro-optical and mechanical properties, AgNWs offer promising performance with electrical conductivity and high transparency as well as mechanical flexibility. CuNWs, while providing similar transparency and conductivity, stand out as a cost-effective alternative due to the lower cost of copper and simpler fabrication processes [25]. Both materials are compatible with various substrates and

deposition methods, though their durability can be enhanced through protective coatings to mitigate oxidation and mechanical instability. With these material properties, they are advantageous in transparent antenna designs. By optimizing the design and using strategic approaches, these nanowires contribute to antennas that maintain high transparency while offering improved radiation efficiency for transparent monopole [26] and patch antennas [27].

In conclusion, the transparency of these materials, in addition to their structural and nanoscale properties in the visible spectrum, is achieved by reducing their thickness to the scale of tens of nanometers. However, such thin conductors, with lower conductivity compared to traditional materials like copper or silver, present a considerable challenge in antenna design. This creates a critical trade-off between achieving high optical transparency and maintaining acceptable radiation efficiency. A detailed exploration of this trade-off and its implications for antenna performance is presented in the next section.

2.2 Challenges in Transparent Antenna Design Regarding Transparency and Radiation Efficiency

Transparent antenna design faces a critical trade-off between achieving high optical transparency and maintaining effective radiation efficiency. This challenge arises due to the skin depth phenomenon, which has an impact in both the visible and RF spectra. In the visible spectrum, optical transparency (or the transmission coefficient, T) is exponentially related to the material's thickness (t) and the skin depth for visible light (δ_v) through the equation [28]:

$$T = e^{-\frac{t}{\delta_v}}. \tag{2.1}$$

This relationship indicates that higher transparency requires thinner conductive materials with today's technology and the known materials. The skin depth for visible light is primarily determined by material properties, such as electron relaxation time and electron concentration. Consequently, unless there is a breakthrough in material science, achieving higher transparency necessitates thinning the conductor, often to the nanoscale. Transparent conductors typically have thicknesses in the range of a

few tens of nanometers; for example, silver nanowire films achieve approximately 80% transparency at a thickness of around 200 *nm*.

In RF spectrum, effective radiation needs good conductivity, which requires a material thickness significantly greater than the skin depth (δ) for RF, which is given by

$$\delta = \sqrt{\frac{1}{\pi f \mu \sigma}}, \tag{2.2}$$

where f is the operating frequency, μ is the magnetic permeability, and σ is the conductivity. For RF applications, even the skin depth of highly conductive materials like silver is much greater than the thickness of typical transparent conductors. To illustrate, the skin depth for solid silver ($\sigma \approx 63 \times 10^6\ S/m$) at 3.5 GHz is around 1 μm, while the one for ITO ($\sigma \approx 10^6\ S/m$) at 3.5 GHz is approximately 8.5 μm, which indicates the substantial disparity compared to 200 nm.

Since transparent conductors generally have lower conductivity than bulk silver, their limited thickness further exacerbates their loss resistance. This significant loss resistance negatively impacts antenna radiation efficiency, presenting a fundamental challenge for designing efficient transparent antennas.

2.3 Surface Resistance

In practice, determining the precise conductivity or thickness of transparent conductors can often be challenging. This difficulty is particularly pronounced in materials such as multilayer TCOs or randomly distributed silver nanowire networks, where structural inhomogeneity complicates direct measurement. To address this, the surface resistance parameter, which accounts for both conductivity and thickness, is widely used as a practical metric to characterize transparent conductor films.

Surface resistance (R_s) quantifies the resistance encountered by electric current flowing along the surface of a material. It is particularly relevant for thin conductive films and two-dimensional materials, which are often used in applications such as frequency selective surfaces, transparent conductive films (e.g., touchscreens), transparent antennas, and other technologies employing thin metal layers.

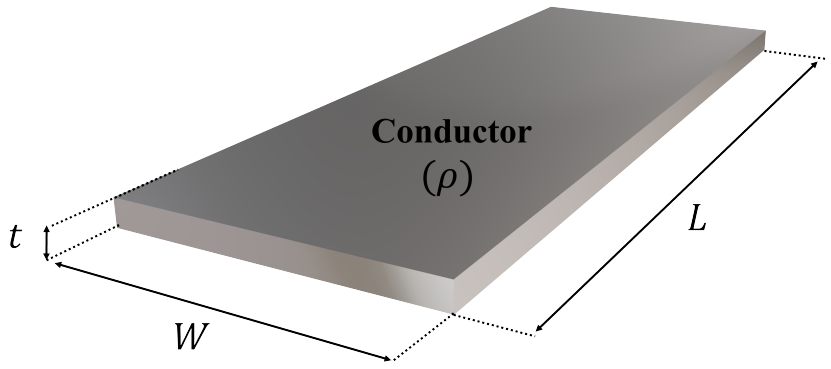

Figure 2.4: Sufficiently thin conductor geometry.

For a sufficiently thin conductor depicted in Fig. 2.4, which has a thickness smaller than the skin depth, the resistance (R) along its length (L) can be calculated using the well-known Ohm's law as follows:

$$R = \rho \frac{L}{tW}, \tag{2.3}$$

where ρ $(\Omega.m)$ is the resistivity, W (m) is the width, and t (m) is the thickness of the conductor sheet. Here, surface resistance is defined as

$$R_s = \frac{\rho}{t} = \frac{1}{\sigma t}. \tag{2.4}$$

It should be noted that R_s has the same unit as resistance (R). Therefore, to distinguish it and specify that it is a surface-related quantity, by adding a square, the notation $\Omega\square$ is used as the unit of surface resistance.

For the sake of generality, considering that the effective thickness is the skin depth at high frequencies, R_s definition can be extended to:

$$R_s = \begin{cases} \dfrac{1}{\sigma t} \ , & t < \delta \\ \dfrac{1}{\sigma \delta} \ , & t > \delta \end{cases} . \tag{2.5}$$

It should be noted that surface resistance is independent of frequency in the RF spectrum since the typical thickness of a known transparent conductor film is smaller than the skin depth, as mentioned earlier.

2.4 Transparent Conductive Nanowires: Material Preparation and Characterization

Conductive nanowire networks, particularly silver nanowire and copper nanowire networks, offer advantages in cost, speed of development cycle, and ease of deposition compared to conventional transparent conductors like ITO or multilayer IZTO/Ag/IZTO.

While the production of transparent metal oxides like ITO is well-developed, it typically requires specialized facilities, such as clean rooms and magnetron sputtering devices. Additionally, the conductivity of the transparent coating can be affected by factors like processing temperature, which restricts the types of materials on which it can be deposited. For instance, flexible substrates like polyethylene terephthalate (PET) may not tolerate the high temperatures needed for ITO deposition to achieve low surface resistance. Lowering the temperature to accommodate these substrates can reduce the conductivity of ITO, making it unsuitable for antenna applications on such substrates.

AgNWs and CuNWs, on the other hand, offer a significantly simpler production process. CuNWs are especially cost-effective due to the lower price of copper compared to silver and the use of water as the solvent during their preparation. These nanowires can be applied to various substrates, such as glass, plexiglass, and PET, using techniques like inkjet printing, screen printing, or even simple spray painting.

AgNWs are synthesized using a modified polyol method as described in prior research, [29]. In this process illustrated in Fig. 2.5, ethylene glycol (EG) serves as both the solvent and reducing agent, silver nitrate ($AgNO_3$) provides the silver source, sodium chloride acts as the nucleating agent, and polyvinyl pyrrolidone (PVP) stabilizes the system to ensure unidirectional growth of the nanowires. The resulting AgNWs are purified through centrifugation and applied to substrates via spray coating

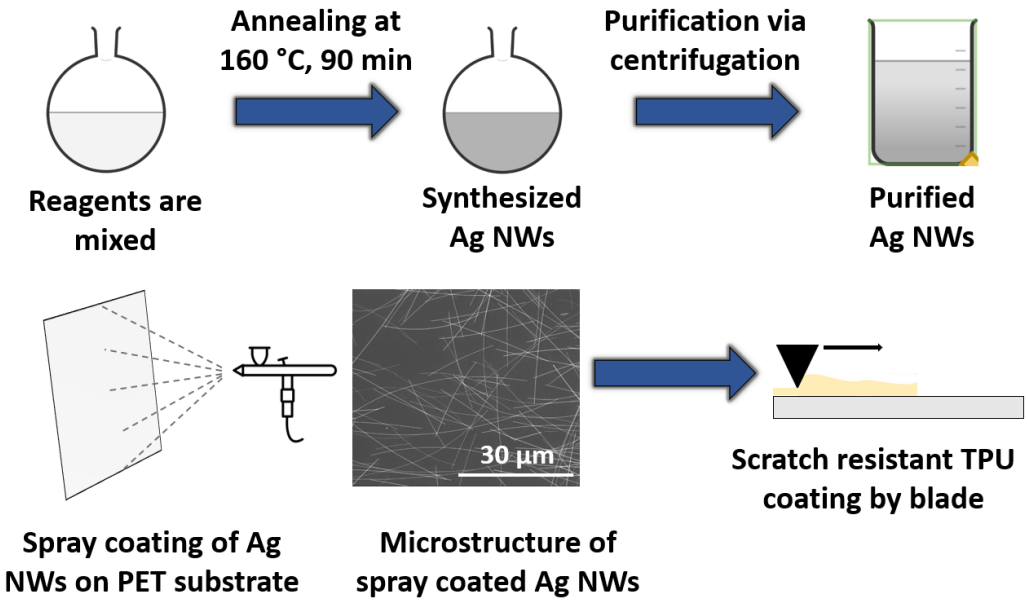

Figure 2.5: AgNW material preparation cycle.

with an airbrush. Post-deposition treatments are conducted to enhance the surface resistance of the AgNW networks.

CuNWs are synthesized using a hydrothermal process, as outlined in [30]. In this method, water acts as the solvent, $CuCl_2$ serves as the copper source, glucose functions as the reducing agent, and hexadecylamine is used as the stabilizing agent. The resulting CuNWs are purified through centrifugation and the removal of byproducts via decantation. Similarly, these nanowires are deposited using the spray coating technique, followed by a post-deposition treatment to lower the surface resistance.

Once AgNW or CuNW coatings are applied to a substrate, they are typically encapsulated with thermoplastic polyurethane (TPU) to enhance scratch resistance and extend their shelf life.

The surface resistance of AgNW and CuNW samples is determined using Signatone Pro4 based on 4-point probe method, which is connected to a Keithley 2400 sourcemeter. Their optical transmittance (or transparency) is measured using the Shimadzu UV-3600 UV-Vis-NIR spectrophotometer. Fig. 2.6 shows the optical transparency measurements, where the terms "thin" and "thick" correspond to the coating thickness of the samples. The thickness of AgNW networks is not easily determined

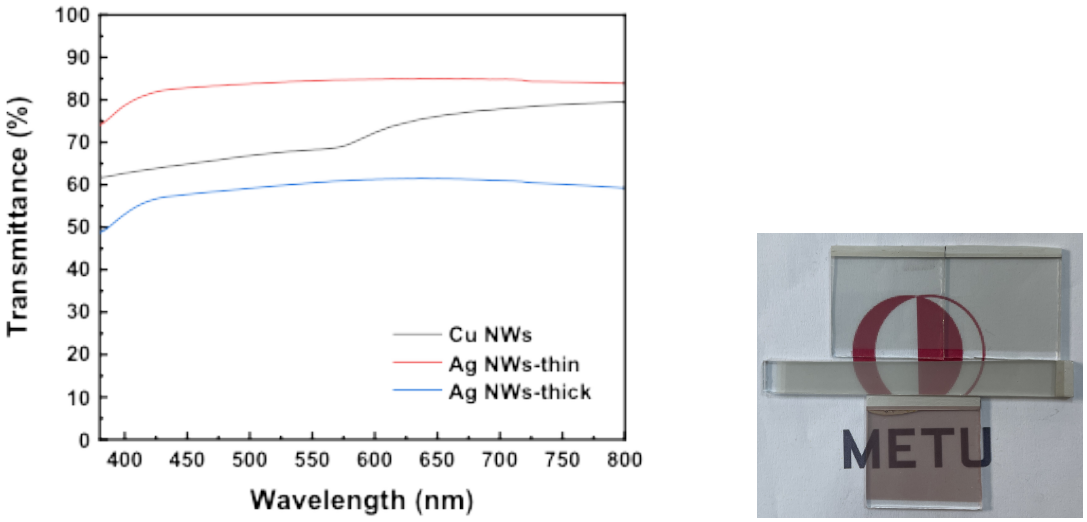

(a) (b)

Figure 2.6: AgNW and CuNW films: (a) measured optical transmittance, (b) fabricated samples.

or measured due to their microstructure as seen in Fig. 2.5 but is given approximately. A thicker AgNW (approximately 350-400 *nm*) coating can achieve a surface resistance of 6 Ω□ with 60% transparency at 550 *nm*, while the thinner (approximately 200 *nm*) provides more than 80% transparency with a surface resistance of 10-12 Ω□. On the other hand, dense CuNW networks can achieve surface resistances of less than 10 Ω□ while maintaining an optical transmittance of 68% in average.

Silver nanowire films offer superior transparency compared to their copper nanowire counterparts, making them ideal for applications where optical clarity is a priority. However, CuNW films stand out for their lower cost and environmentally friendly production process, often referred to as a "green" alternative. Despite these advantages, CuNWs are prone to rapid degradation, which results in increased surface resistance and unstable radiation efficiency over time. Even though they are covered with TPU to avoid oxidization, remaining air under TPU during preparation leads to a degradation up to some extend; and then saturates. This shorter shelf life limits their long-term reliability. Encouragingly, advancements in material science are being made to address these limitations, focusing on methods to enhance the stability and durability of CuNWs.

The transparent monopole and patch antennas designed in this thesis work are prototyped using AgNW coated PET films. They are fabricated with the production process stated above by Nanovatif Materials Technologies and the Department of Metallurgical and Materials Engineering, METU. AgNWs are airbrushed on 0.127 *mm*-thick PET films and covered with TPU. The samples are scratch resistant and mechanically flexible. Most significantly, they have more than 80% optical transparency with approximately 10 $\Omega\square$ surface resistance.

CHAPTER 3

ANALYSIS AND DESIGN OF HIGHLY TRANSPARENT AND EFFICIENT FLEXIBLE MONOPOLE ANTENNA

3.1 Introduction

The seamless integration of transparent antennas into surfaces such as windshields or glass frames has gained significant attention in recent years due to their potential applications in vehicular communication systems, smart windows, and wearable devices. However, achieving an optimal balance between optical transparency, antenna efficiency, design simplicity, and cost-effective fabrication methods remains a considerable challenge. Transparent antennas, typically made from conductive films, often exhibit low efficiency unless enhanced through multilayered structures or increased film thickness, which can compromise transparency or raise manufacturing costs.

This chapter explores these challenges by addressing the fundamental trade-offs in designing a highly transparent monopole antenna and proposes solutions to overcome these limitations. Specifically, it introduces a simple yet effective monopole antenna topology, identifies key factors affecting antenna performance, and demonstrates reliable, low-cost fabrication techniques. The main contributions of this research are summarized as follows:

1. The proposed antenna is designed for deposition on thin, flexible substrates such as Parylene C or polyethylene terephthalate (PET). Its single-sided geometry incorporates a monopole antenna excited by a coplanar waveguide (CPW), eliminating the need for a ground plane typically required by microstrip patch antennas. This configuration enables convenient integration onto various surfaces, including glass, as a flush-mounted or sticker-like solution.

2. Conventional transparent antennas often rely on fabrication methods such as photolithography or sputtering, which are costly and impractical for large-scale production. In contrast, the antennas developed in this chapter utilize silver nanowire networks and are fabricated using accessible methods stated in Ch. 2. These approaches bypass the need for clean room operations, significantly reducing production costs.

3. A comprehensive study is conducted to identify and address the limiting factors affecting antenna efficiency. Strategies for improving performance while maintaining transparency are discussed in detail, ensuring practical applicability for real-world deployment.

4. The conventional approach to achieving optical transparency involves using extremely thin conductive films (e.g., < 200 *nm*). Thus, simulating such thin films accurately in electromagnetic (EM) simulation software can be challenging. This chapter also presents two methodologies: one employs setting mesh resolution for 3D thin solid geometries, while the other utilizes a 2D impedance boundary surface. The two methods yield matching results.

After these discussions and analyses, the finalized transparent monopole designs are fabricated and measured to validate the proposed methods and designs. The chapter concludes with the presentation of key performance metrics, including *S*-parameters, gain, and radiation pattern measurement results, providing an evaluation of the prototypes' practical performance.

3.2 Planar Monopole Antenna Geometry

As stated in Ch. 2, thin transparent conductors inherently exhibit limited electrical conductivity. To address this limitation, one effective approach can be to minimize reliance on such materials in the antenna design. For instance, patch antennas require both the radiator and the ground plane to be transparent, which means that this configuration brings more losses associated with the thin conductive films, as addressed in Ch. 4.

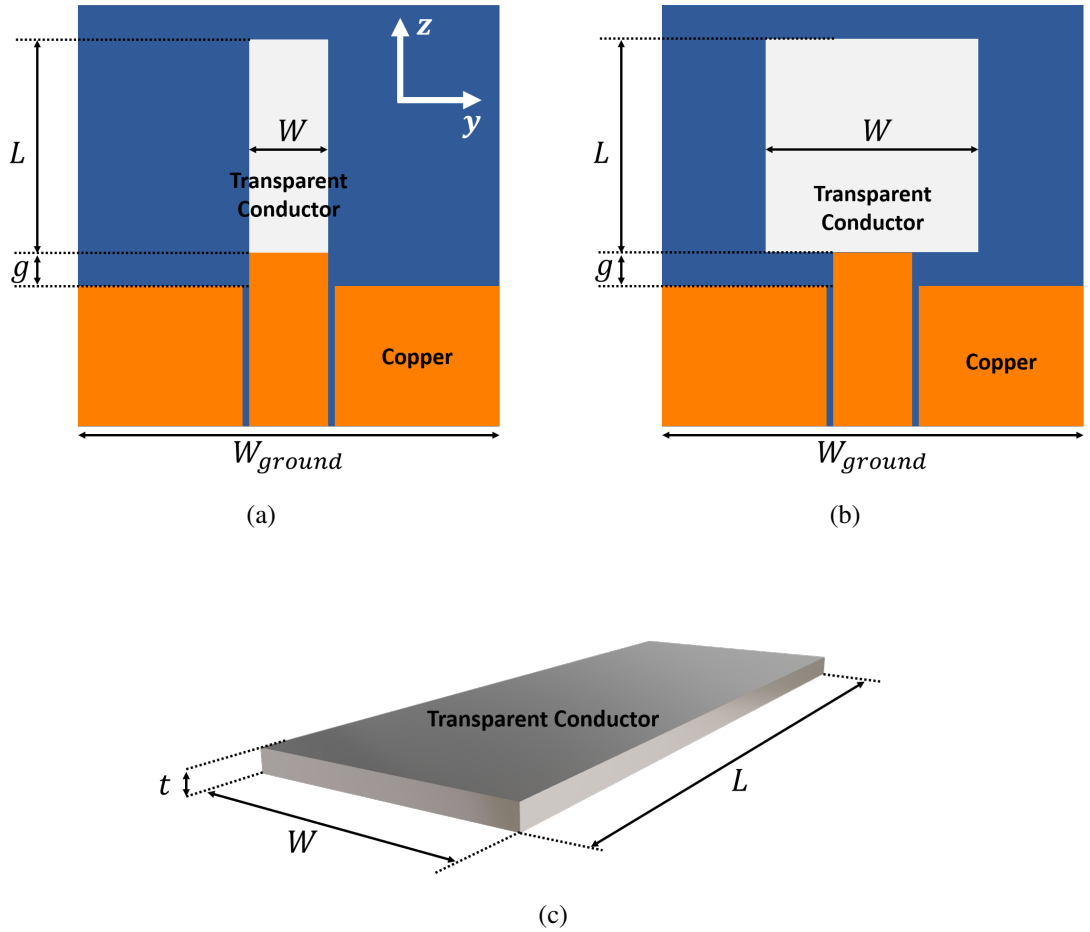

Figure 3.1: Design parameters of the antennas: (a) narrow monopole, (b) wide monopole and (c) the geometry of transparent conductor part.

In this research, a planar monopole antenna geometry is proposed, as illustrated in Fig. 3.1. Unlike patch antennas, this design eliminates the need for a transparent ground plane, significantly reducing the associated losses. The monopole antenna is fed via a coplanar waveguide (CPW), which does not need to be transparent and can conveniently be concealed within the frame of a windshield, window, or glasses.

The key geometric parameters under consideration are the monopole's length (L), width (W), and thickness (t), as depicted in Fig. 3.1. The CPW feed line, constructed from copper and FR4 substrate, introduces a potential gap (g) when the antenna width exceeds the CPW's line width as in Fig 3.1b. Transparent conductor is placed on PET film, which has a thickness of 125 μm, providing a support for the antenna.

3.3 Radiation Efficiency and Gain Reduction in Planar Monopole Antennas

Directivity (D) refers to the ability of an antenna to concentrate radiated power in a particular direction, while gain (G) accounts for both directivity and the efficiency of the antenna in transforming input power into radiated power. The relationship between these two parameters is given by

$$G = e_r D, \tag{3.1}$$

where e_r is the radiation efficiency. It is calculated from

$$e_r = \frac{R_{rad}}{R_{rad} + R_{loss}}, \tag{3.2}$$

where R_{rad} is the radiation resistance and R_{loss} is the loss resistance which includes all dielectric, conductor, and surface wave loss in the antenna. For optically transparent antennas, the majority of the loss comes from the lossy transparent conductor. Particularly, in transparent conductor part of the monopole antenna in Fig. 3.1, dielectric loss is ignorable and the surface wave loss is irrelevant. Considering that the monopole has a geometry shown in Fig. 3.1c, the loss resistance can be calculated as

$$R_{loss} = kR_s\frac{L}{W}, \tag{3.3}$$

similar to (2.3). Here, k is a unitless constant which can be taken as 0.5 for a sinusoidal current distribution at RF frequencies [31]. To validate the loss resistance calculation and thus the efficiency, regular planar monopole antennas over a finite ground plane shown in Fig. 3.2 are examined at 3.5 GHz and 5.9 GHz. The dimensions of the interested monopoles are $L = 19.9\ mm$, $W = 1\ mm$ at 3.5 GHz and $L = 11.65\ mm$, $W = 1\ mm$ at 5.9 GHz. Both antennas are simulated using full wave EM simulator for a range of possible surface resistances up to 10 $\Omega\square$.

Directivities of the planar monopoles are simulated and found to be 2.5 dBi at 3.5 GHz and 2.67 dBi at 5.9 GHz. Radiation resistance is 36 Ω. Fig. 3.3 shows the gain simulated and calculated by (3.1–3.3) for both operational frequencies. It is seen that the basic loss resistance calculation can well predict the radiation efficiency and gain reduction for a thin planar monopole antenna.

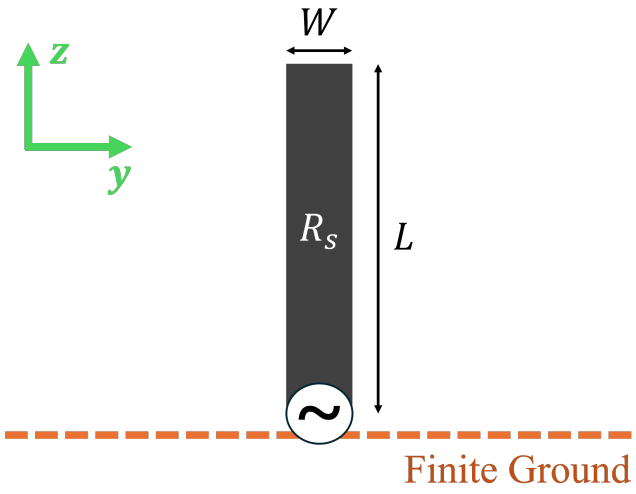

Figure 3.2: Generic planar monopole geometry over a finite ground.

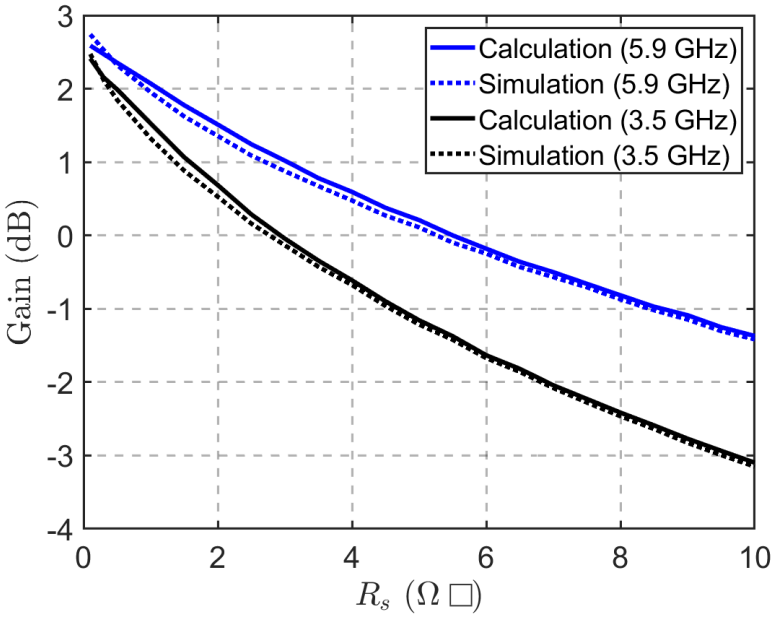

Figure 3.3: Calculated and simulated antenna gains of two generic planar monopoles at 3.5 GHz and 5.9 GHz.

The surface resistance has an impact that it can significantly reduce the antenna gain at 3.5 GHz by approximately -5.5 dB resulting from the radiation efficiency of 28% when it is 10 Ω□. At 5.9 GHz, the gain reduction is around -4 dB with the radiation efficiency of 39%, which is higher than the one at 3.5 GHz. This is naturally because the conductor length is shorter, making the loss resistance smaller when the width is kept the same. This also shows that the antenna is less efficient at lower frequencies.

To improve the gain and to have an efficient antenna, surface resistance should be lowered, the operational frequency can be increased, leading to a shorter conductor generally. However, R_s depends on the material and it is usually a fixed number once the thin film or coating is produced. The frequency might be limited to the requirements of antenna applications. At this point, it is clear from (3.2) that making W wider improves the efficiency, and accordingly this research proposes a wide flat monopole as shown in Fig. 3.1b.

3.4 Simulation Environment and Reliable Modeling

The monopole antennas in this research are analyzed using a FEM based solver. Firstly, all the structure is created as 3D solid objects. Since the transparent part has a thickness of 200 nm or less, which is very thin compared to the rest of the FEM solution space, it may not be meshed effectively. For a better meshing and more accurate solution, mesh operation is assigned to the transparent conductor by adjusting the model resolution as in the order of nanometers, which may lead to a larger numbers of mesh elements and more memory needed.

Another method is to use impedance boundary condition (IBC). The transparent part is created as a 2D sheet and the surface resistance, which can be measured or calculated considering the thickness and bulk resistivity, is assigned to it.

It is observed that both 2D and 3D solutions of a transparent planar monopole antenna yield the same reflection coefficient (Fig. 3.4), input impedance and gain results for 100, 50, and 20 *nm* thick conductor with a 10^6 S/m conductivity, which means the surface resistances are 10 Ω□, 20 Ω□, and 50 Ω□, respectively.

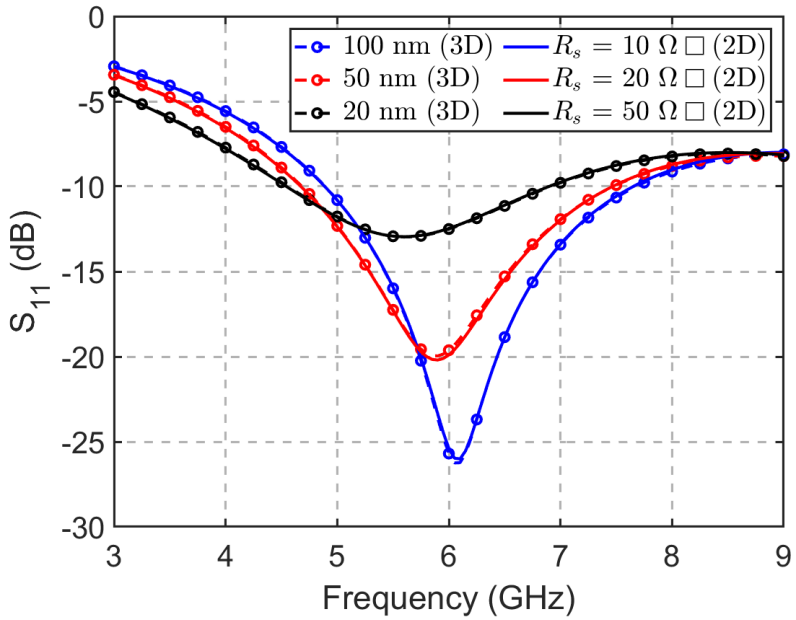

Figure 3.4: Simulated S parameters of transparent planar monopole antenna when represented by a 3D solid object with very thin thickness and 2D sheet on which its surface resistance is assigned.

In some fabrication processes, unlike ITO films, the thickness of silver nanowire coating is more difficult to determine due to the surface roughness or complex alignment of the nanowires. In this case, for 3D solution method, an average thickness value and the bulk conductivity can be considered but the simulation results might differ from the measurement. Instead, it is more convenient to use the 2D method since the surface resistance of silver nanowire can be measured easily. Accordingly, all the analyses are performed by using 2D method throughout the research.

3.5 Effects of Design Parameters

In this section, design parameters of CPW-fed planar monopole antenna in Fig. 3.1 are examined in terms of input impedance and radiation efficiency focusing on the operational frequency of 5.9 GHz. Simulations are carried by using impedance boundary for the transparent part as outlined above. The line width of the CPW line on 1.5 *mm*-thick FR4 is 2.8 *mm*, which constitutes to 50 Ω characteristic impedance.

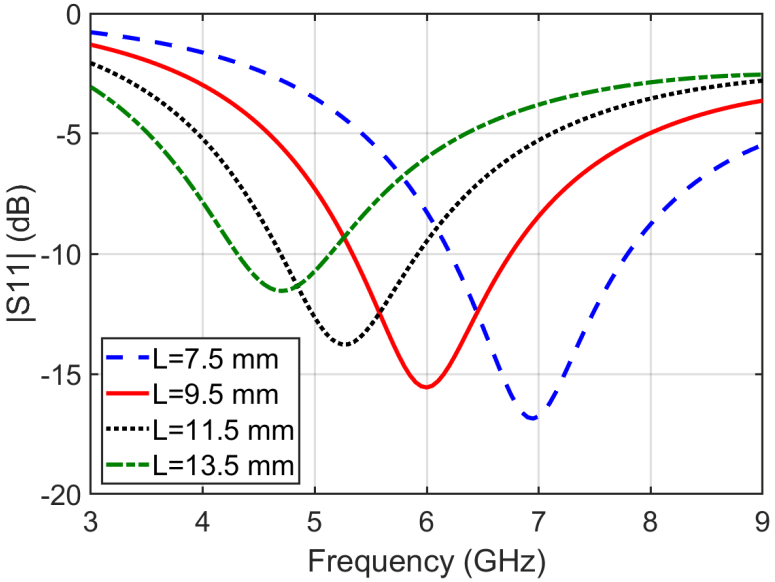

Figure 3.5: Reflection coefficients for various monopole width L when $R_s = 10\ \Omega\square$.

Since the direction of currents is in alignment with the longitude of the monopole, the length L is effective on the operational frequency, and it is at the vicinity of a quarter wavelength. As L is increased, the resonance frequency shifts to lower frequencies as expected and seen in Fig. 3.5. Keeping the width ($W = 2.8\ mm$) and the gap ($g = 0.7\ mm$) constant, the same monopole antenna is simulated when it is assigned separately as PEC and transparent ($R_s = 10\ \Omega\square$) at 5.9 GHz. The input impedance of the monopole is given in Fig. 3.6, where one can see the difference in the real parts as the loss resistance. Naturally, a greater length gives rise to a higher loss resistance (3.3) and the monopole becomes inductive at the chosen operational frequency. This also shows that the antenna is less efficient at lower frequencies.

As the width W of the transparent monopole is increased keeping the length ($L = 9.5\ mm$) and the gap constant, a better reflection coefficient is obtained as seen in Fig. 3.7. Similarly, the same monopole is simulated for both the PEC and the transparent cases at 5.9 GHz. The input impedance is given in Fig. 3.8. The loss resistance, inferred from the difference in the real parts of the both cases, is reduced with a larger width as expected from (3.3). Particularly, increasing the width from 2.8 *mm* to 9.5 *mm* elevates the radiation efficiency from 68% to 77%. Thus, widening the antenna structure can improve the efficiency without sacrificing optical transparency when

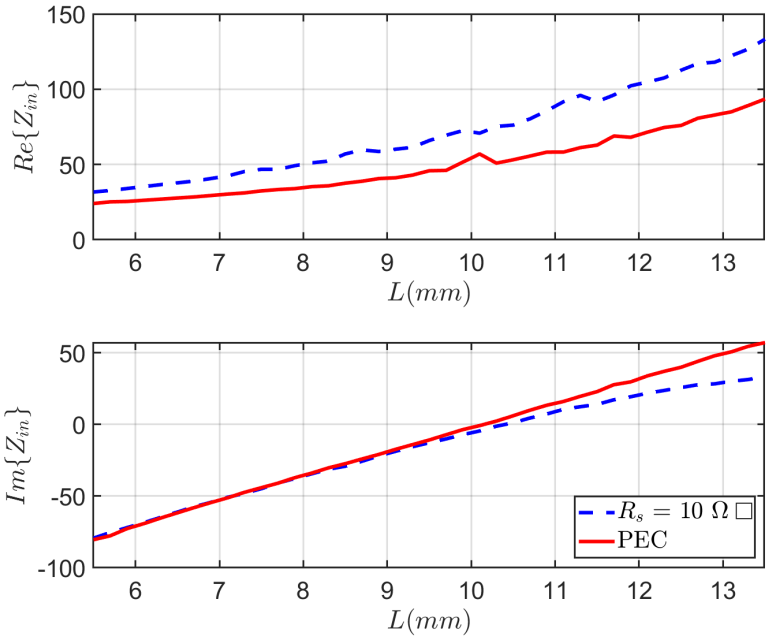

Figure 3.6: Input impedance of transparent and PEC monopoles with respect to the length L at 5.9 GHz.

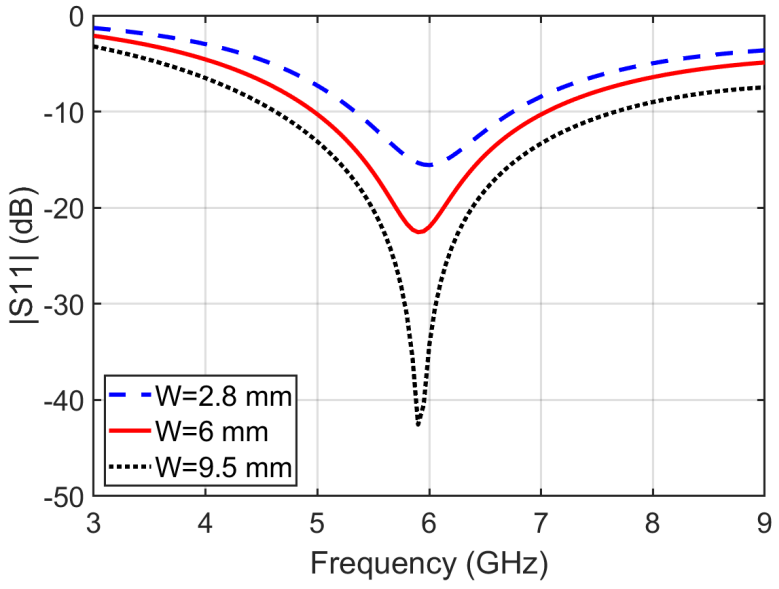

Figure 3.7: Reflection coefficients for various monopole width W when $R_s = 10\,\Omega\square$.

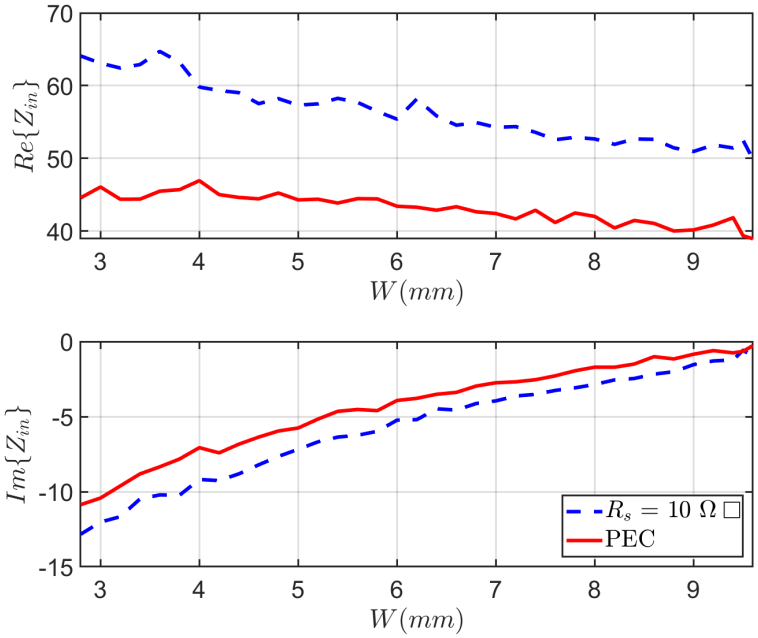

Figure 3.8: Input impedance of transparent and PEC monopoles with respect to the width W at 5.9 GHz.

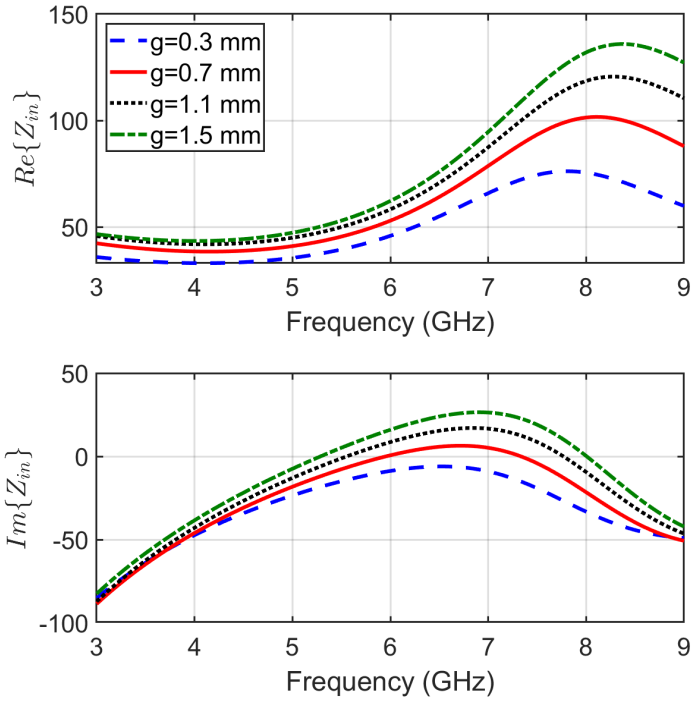

Figure 3.9: Input impedance of transparent monopole for different g values.

considered as percentage only on the conductor region. Moreover, within this range of W, the imaginary part of the input impedance tends to approach 0, which also explains the better resonance behavior. In general, a fat planar monopole antenna lifted off its ground can have wide-band operation when its width and the gap are designed for impedance matching [32].

In addition to the length and width, the gap (g) is studied because it affects the reactance of the antenna's input impedance. A larger gap moves the resonance to lower frequencies as it makes the overall length of the antenna longer. A smaller gap adds a capacitive effect, which reduces the reactance as seen in Fig. 3.9.

3.6 Further Improvement in Gain and Radiation Efficiency

It is presented that the efficiency of the flat monopole antenna designed from transparent conductor can be improved by increasing the width. The current on the transparent monopole is strongly distributed on the bottom and side edges as shown in Fig. 3.10a.

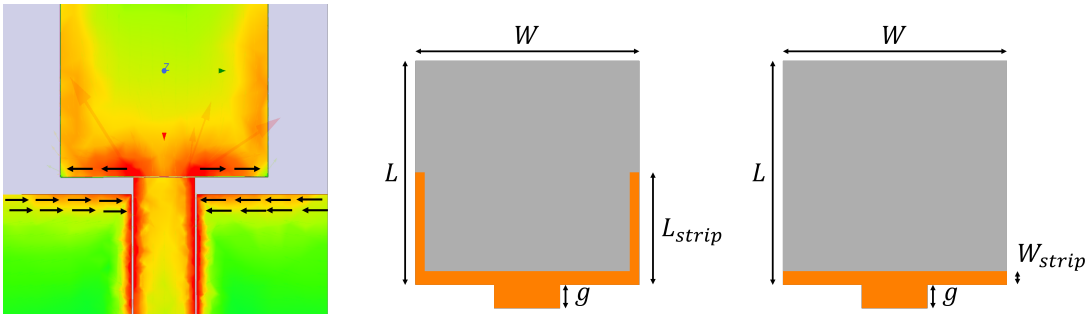

(a) (b)

Figure 3.10: For the square-shaped transparent monopole antenna, (a) current distribution at 5.9 GHz, (b) the geometry of good conductor strips on the bottom and side edges.

The following study is to creatively place better conductors on the monopole to improve its efficiency, similar in nature [33]. Copper strips are placed on the edges of monopole (Fig. 3.10b) where the current density is the highest. The copper strips have a thickness of W_{strip} and the length is L_{strip} on the vertical edges. The bottom edge is

fully framed with the strip. When the vertical strips are extended to half of the transparent monopole ($L_{strip} = L/2$) and have a 0.1 *mm* width, the optical transparency is reduced by 3.5%. The radiation efficiencies at 5.9 GHz for both narrow (W = 2.8 *mm*) and wide (W = 9.5 *mm*) monopole are obtained as 80% and 87%, respectively. Thus, around 10% improvement compared to transparent monopoles without copper strips stated above is achieved by adding tiny strips.

For several vertical strip lengths, the radiation efficiency of the transparent monopole antenna at 5.9 GHz is tabulated in Table 3.1. In general, as the strip length is extended, the efficiency increases. After half of the vertical edge, the rate of the increase is slower. Besides, since the bottom edge has the strongest current distribution, the efficiency improvement due to placing strips only on the bottom edge is greater than the one for extending it in vertical direction. Additionally, the S_{11} parameter does not significantly change when the strip is placed on the bottom edge for this particular monopole, as seen in Fig. 3.11. Thus, one can consider that it is reasonable to design wide transparent monopole antenna by adding a tiny horizontal strip only on the bottom edge to have a minimum sacrifice of optical transparency.

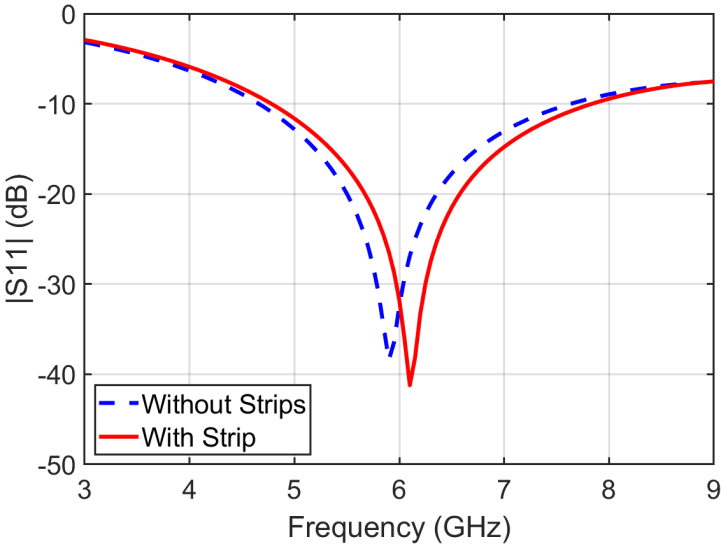

Figure 3.11: S_{11} for the monopoles with and without the bottom strip.

Table 3.1: Radiation Efficiencies for Different Lengths of the Vertical Copper Strips at 5.9 GHz

Strip Length, L_{strip}	$0.0L$	$0.2L$	$0.4L$	$0.6L$	$0.8L$	$1.0L$
Radiation Efficiency	84.1%	85.2%	86.8%	87.5%	88.8%	88.9%

3.7 Cross Polarization

The radiation patterns of the transparent square monopole antenna at 5.9 GHz are similar to that of a dipole antenna except the cross-pol pattern in H plane (Fig. 3.12). The cross-polarization level has been observed to be below -20 dB in all planes except for H plane on which there is a lucky clover-shaped cross polarization and it is affected by the ground width W_{ground}. This is due to the horizontal current induced on the top edges of the CPW grounds. Cross polarization patterns on H plane for different ground widths can be observed in Fig 3.13a. The cross-pol levels normalized to the maxima of the co-polarizations are given in Table 3.2. As W_{ground} is increased, the cross-polarization level gets larger. After the ground is increased to a significant value when it is effectively seen as infinite, the cross-pol component disappears as in the case of quarter wavelength monopole.

Tapering the grounds of CPW as depicted in Fig. 3.13b alters the current distribution on the grounds of CPW line, and consequently reduces the cross polarization. For 30 mm ground width, the tapering results in -16.3 dB cross-pol level. Therefore, a 5.4 dB improvement (compared to Table 3.2) in cross-pol can be achieved.

Table 3.2: Normalized Cross-Polarization Levels at 5.9 GHz

Ground Width (W_{ground})	**20 mm**	**30 mm**	**40 mm**
Cross-Pol Level	-19.1 dB	-10.9 dB	-5.6 dB

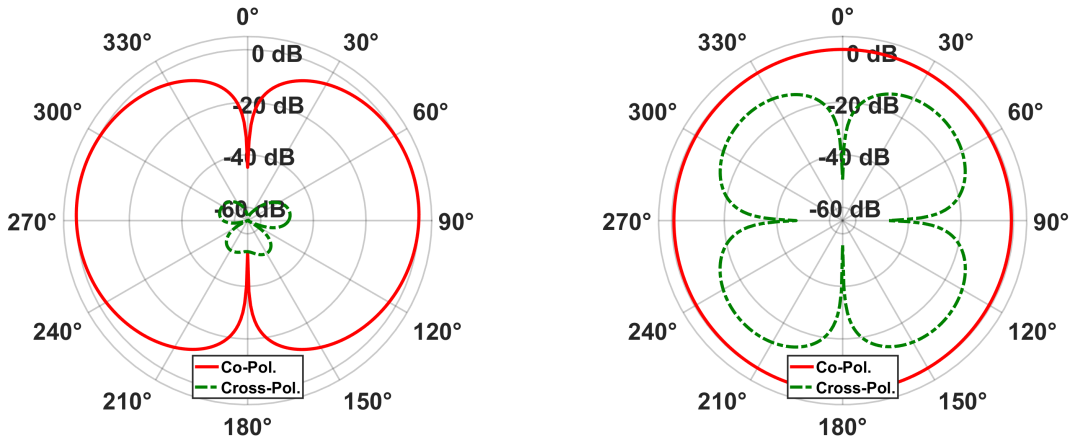

(a) (b)

Figure 3.12: Radiation patterns of the transparent square monopole antenna at 5.9 GHz: (a) E plane, (b) H plane.

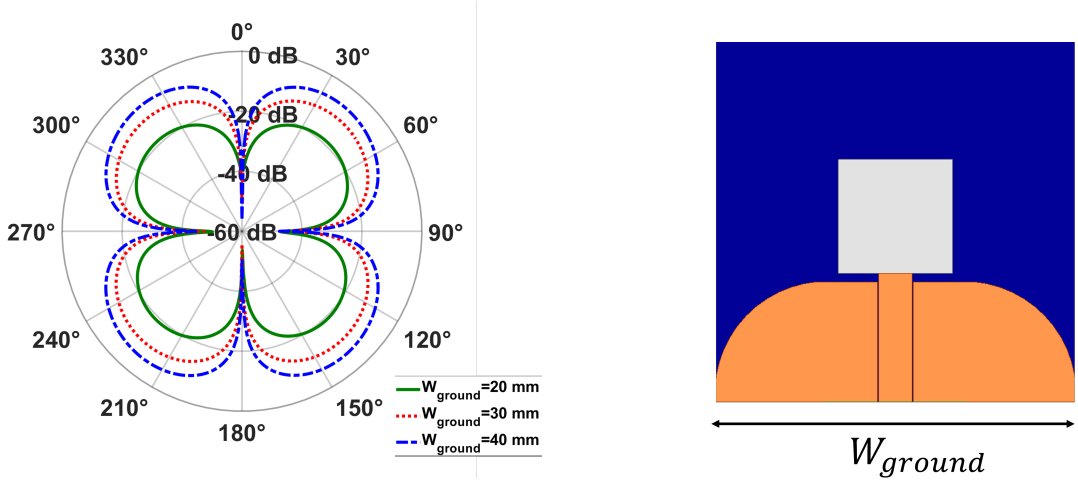

(a) (b)

Figure 3.13: (a) Cross polarization patterns in H plane for different ground widths at 5.9 GHz, (b) tapered ground geometry to enhance the cross-pol level.

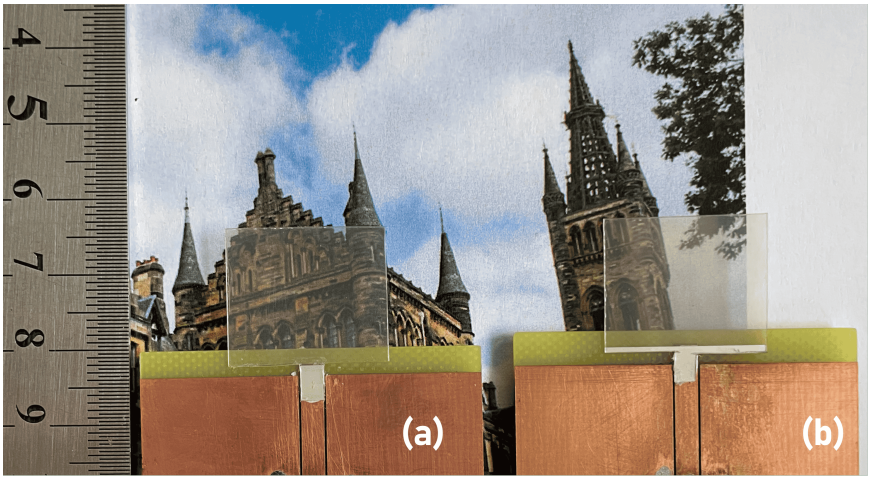

Figure 3.14: AgNW monopole antennas fed by CPW line: (a) Prototype I without silver strip, (b) Prototype II with silver strip at the bottom.

3.8 Proposed AgNW Transparent Monopole Antennas, Fabrication, and Measurements

Following the studies discussed in this chapter, two wide planar monopole antennas ($L = 18$ *mm*, $W = 21$ *mm*) are designed at 3.5 GHz. Prototype I has the same geometry as seen in Fig. 3.1b. Prototype II consists of a thin silver (highly conductive) strip on the bottom edge. Since the width and the gap have impact on the impedance matching, the antennas have wideband behavior covering both 3.5 GHz and 5.9 GHz, which are allocated for 5G and V2X communications, respectively.

AgNW films are prepared as outlined in Ch. 2. While preparing them, a contact point is placed for the connection between AgNW and the feed line. Besides, the bottom strip of Prototype II is also created similarly to the contact point. On the other hand, the CPW line is fabricated with 1.5 *mm*-thick FR4 substrate by using LPKF machine. Its line width is 3 *mm* and the gap between the line and the ground is 0.3 *mm*. AgNW monopoles and the feed line are connected to each other through the contact points by using a low temperature silver paste, which is cured at around 100°C for 30 minutes. The final prototypes are as shown in Fig. 3.14.

The measured S_{11} results of the two transparent monopole prototypes are given in Fig. 3.15. Measured S_{11} of the monopole without strip is in line with the simulation.

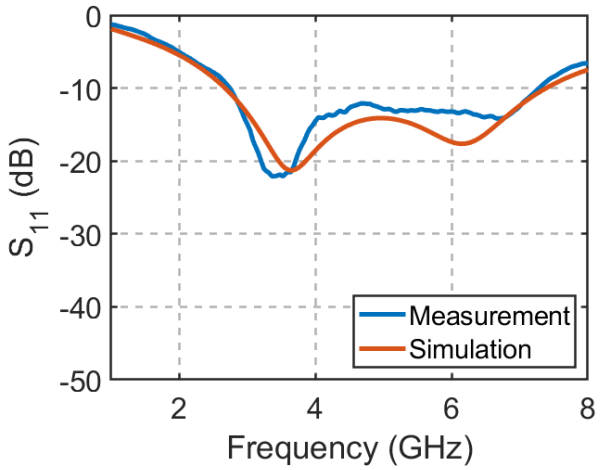

(a)

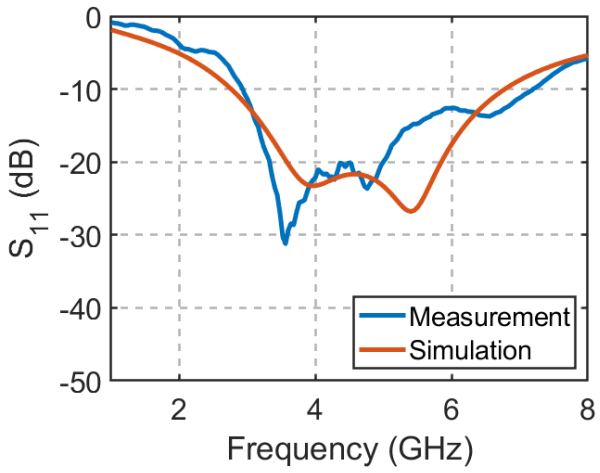

(b)

Figure 3.15: Simulation and measurement results of S_{11}: (a) Prototype I without silver strip, (b) Prototype II with silver strip at the bottom.

Although the bandwidth is similar, the measured S_{11} of the monopole with the bottom strip slightly differs from the simulation. This might be due to reasons related to the fabrication such as misalignment or the distribution of silver paste.

Table 3.3: Simulated and Measured Antenna Gains for the AgNW Monopole Antenna Prototypes Fed by CPW Line at 3.5 GHz.

		Gain (dBi)	Efficiency
Prototype I	Sim.	-0.01	70%
	Meas.	-1.39	50.4%
Prototype II	Sim.	0.79	84%
	Meas.	0.36	76.3%

Gain and radiation pattern measurements are conducted in the anechoic chamber to evaluate the performance of two antenna prototypes. As seen in Table 3.3, for Prototype I, the measured gain is -1.39 dB, with an efficiency of 50.4%. In contrast, Prototype II demonstrates a significant improvement, achieving a measured gain of 0.36 dB and an efficiency of 76.3% with only 5% loss of optical transparency. It should be noted that the simulated results slightly differ. This is mainly because the low-temperature silver paste used to connect the AgNW to the CPW line is not stable in homogeneity and conductivity when it is not properly cured.

The radiation patterns in the principle planes are given in Fig. 3.16. In general, the co-polarization patterns for both antennas are approximately the same as the simulations. On the other hand, although there are slight differences, the lucky clover shape can be observed in the cross-pol patterns in H plane. The cross-pol patterns in E plane has a difference from the simulations in $\phi = 0^\circ$ cut. This is due to the misalignment of the monopoles when measured in the chamber. Indeed, the simulated patterns in the neighboring $\phi = \pm 10^\circ$ display a larger cross-pol level as well. Thus, the angle of placement during the measurement leads to this difference in E plane cross-pol level.

In conclusion, the developed AgNW monopole antennas demonstrate remarkable performance in terms of efficiency and optical transparency. Prototype II achieves a significant improvement with an efficiency of 76.3%, while maintaining an optical transparency exceeding 80%.

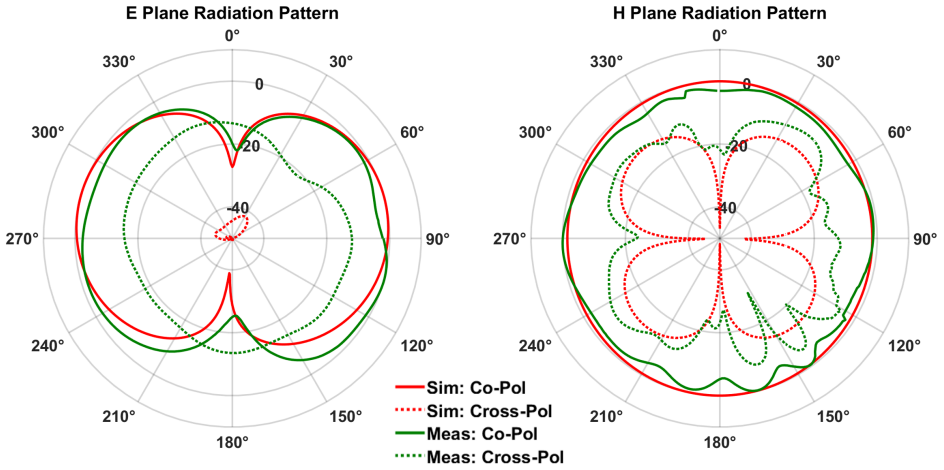

(a)

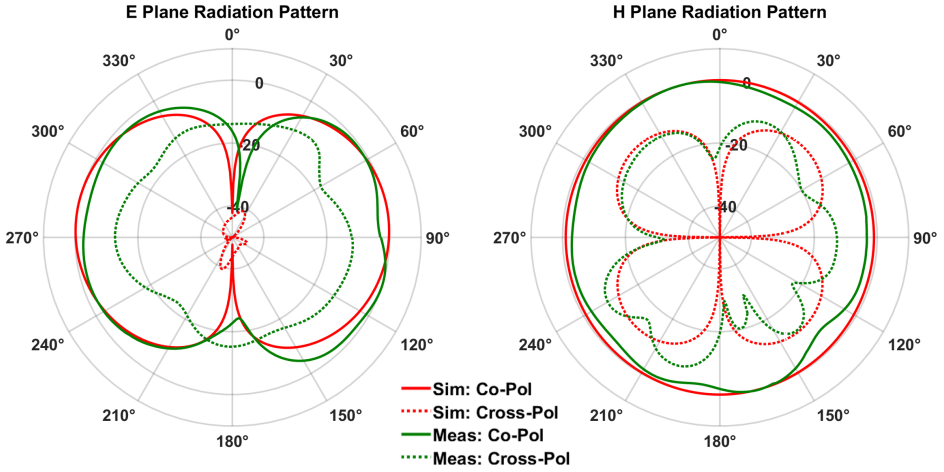

(b)

Figure 3.16: Simulation and measurement results of radiation patterns in principle planes at 3.5 GHz: (a) Prototype I without silver strip, (b) Prototype II with silver strip at the bottom.

CHAPTER 4

ANALYSIS AND DESIGN OF OPTICALLY TRANSPARENT AND EFFICIENT PATCH ANTENNA

4.1 Introduction

Microstrip patch antennas are desirable in many applications where seamless integration is demanded. The properties that traditional patch antennas provide, such as unidirectional pattern and conveniency in array configurations, make them preferred. However, the challenge in balancing transparency and radiation efficiency still exists. Previous studies have shown different methods to achieve optical transparencies [2], but all of them either involve a visually perceptible meshed conductor or have very low gain. The latter is particularly accentuated when a patch antenna is made transparent for both the radiator and its ground plane, which puts more difficulty when compared to a transparent monopole antenna as designed in Ch. 3. The study presented in this chapter examines the underlying principles contributing to the radiation efficiency and subsequently proposes methods to improve the gain of a transparent conductive patch antenna made of AgNW films.

4.2 Analysis of Loss Factors in Transparent Patch Antennas

An antenna made from any transparent conductor suffers from reduced efficiency. This is because a conductor is processed to be very thin (e.g. less than 0.05 of a microwave skin depth at 10 GHz) in order to achieve optical transparency, and therefore it presents a relatively high Ohmic loss. In order to propose methods for improvements, main factors contributing to a gain reduction for a patch antenna are analyzed.

The geometry of the antenna under examination is shown in Fig. 4.1.The patch conductor is very thin (smaller than the skin depth), and represented by a surface resistance R_s ($\Omega\square$). It is placed above a PEC ground plane with a dielectric spacer.

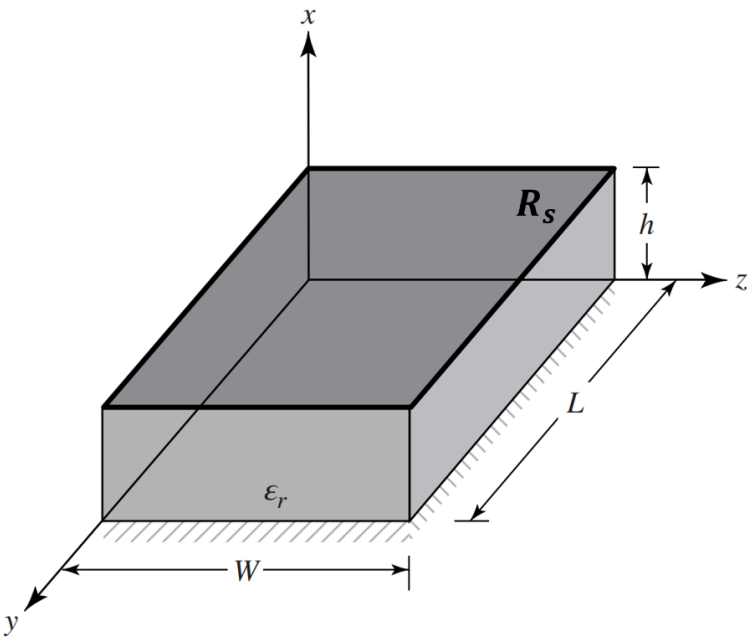

Figure 4.1: Lossy conductor rectangular patch antenna geometry.

4.2.1 Attenuation Due to Surface Resistance of a Radiating Patch

This study follows the transmission line model of a patch antenna. Treating the antenna as a parallel plate transmission line, the complex propagation constant is written as

$$\gamma = \sqrt{(R' + j\omega L')(G' + j\omega C')} = \alpha + j\beta, \tag{4.1}$$

where α and β are the attenuation and the phase constants, and R', L', G', C' are the unit length resistance, inductance, conductance, and capacitance, respectively. The loss tangent of the dielectric substrate is assumed to be low to allow $G' \approx 0$, and the rest of the unit length values can be readily written using the parallel plate transmission distributed element as

$$R' = \frac{R_s}{W}, \quad C' = \epsilon\frac{W}{h}, \quad L' = \mu\frac{h}{W}, \tag{4.2}$$

where R_s is the surface resistance of the radiating element, h is the substrate thickness, W is the width of the patch, and ϵ, μ are the permittivity and permeability of the substrate. Then, the attenuation constant can be found as

$$\alpha \approx \frac{R_s}{2h\eta}, \tag{4.3}$$

where η is the intrinsic impedance of the substrate. Over the length of the patch L, the fields are exposed to a conductor loss by $e^{-\alpha L}$.

4.2.2 Directivity Analysis of Lossy Patch Antenna

A traditional rectangular patch antenna can be modeled as a two-element array of magnetic dipoles above a ground plane as shown in Fig. 4.2a. In ideal case, since the rectangular radiator patch is a perfect conductor, both magnetic dipoles can be excited strongly. If the patch is a lossy or extremely thin conductor as in the case of transparent conductors, the second dipole is weakly excited when the antenna is fed from one edge. Thus, the transparent patch antenna might be regarded as a lossy two-element array to investigate the effect of transparent conductors in the directivity.

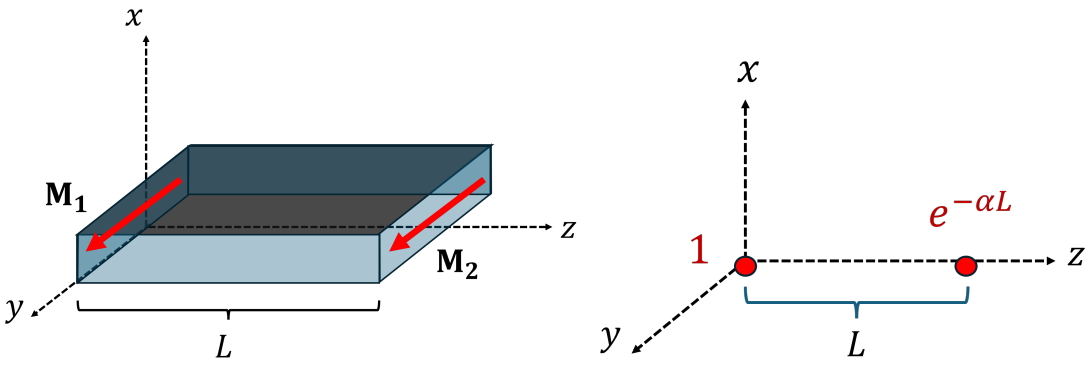

(a) (b)

Figure 4.2: (a) Magnetic current densities and (b) the lossy two-isotropic-element array configuration.

To be more general, the array configuration (Fig. 4.2b) under investigation is formed by two isotropic elements separated by a distance d along $z - axis$. The second element is lossy, which constitutes a reduced amplitude constant $e^{-\alpha d}$. Also, the elements might be excited with a phase difference. For this case, the array factor is

$$AF = 1 + e^{-\alpha d} e^{j\psi}, \tag{4.4}$$

where $\psi = kd\cos\theta + \beta$. Assuming no phased excitation $\beta = 0$, the maximum of $|AF|$ occurs at $\theta = 90°$. Then, the normalized array factor is

$$AF_n = \frac{|AF|}{|AF|_{max}} = \frac{|1 + e^{-\alpha d} e^{j\psi}|}{1 + e^{-\alpha d}}. \tag{4.5}$$

The radiation intensity can be written as

$$U(\theta) = AF_n^2 = \frac{|1 + e^{-\alpha d} e^{j\psi}|^2}{(1 + e^{-\alpha d})^2}, \tag{4.6}$$

whose maximum at $\theta = 90°$ is $U_{max} = 1$. Then, the directivity of the array can be evaluated using

$$D = \frac{4\pi U_{max}}{P_{rad}} = \frac{U_{max}}{U_0}, \tag{4.7}$$

where U_0 is the average radiation intensity and it is given by

$$\begin{aligned} U_0 = \frac{P_{rad}}{4\pi} &= \frac{1}{4\pi}\int_0^{2\pi}\int_0^{\pi} U(\theta)\sin\theta d\theta d\phi \\ &= \frac{1}{2}\int_0^{\pi} U(\theta)\sin\theta d\theta \\ &= \frac{1}{2(1 + e^{-\alpha d})^2}\int_0^{\pi} |1 + e^{-\alpha d} e^{jkd\cos\theta}|^2 \sin\theta d\theta \\ &= \frac{1}{2(1 + e^{-\alpha d})^2}\int_0^{\pi} [1 + e^{-2\alpha d} + 2e^{-\alpha d}\cos(kd\cos\theta)]\sin\theta d\theta \\ &= \frac{1 + e^{-2\alpha d}}{(1 + e^{-\alpha d})^2}. \end{aligned} \tag{4.8}$$

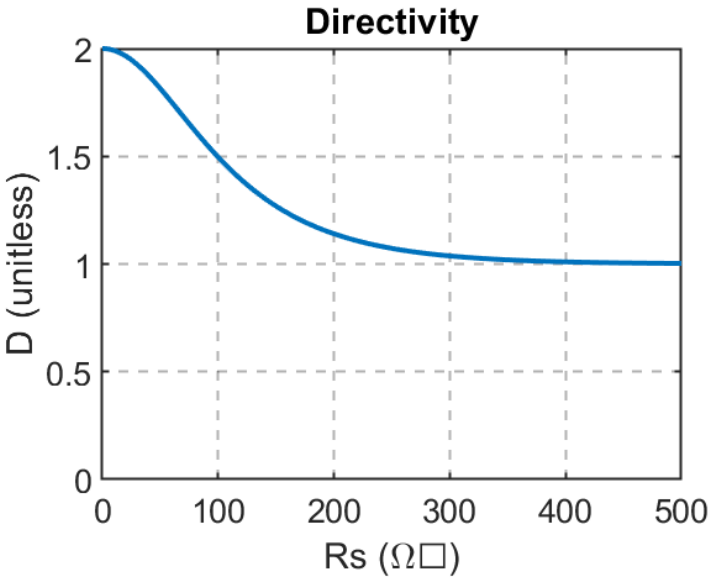

Figure 4.3: Directivity of a rectangular patch antenna at 3.5 GHz with respect to surface resistance.

Using (4.8), the directivity is found to be

$$D = \frac{(1+e^{-\alpha d})^2}{1+e^{-2\alpha d}} = 1 + \frac{2e^{-\alpha d}}{1+e^{-2\alpha d}}. \tag{4.9}$$

For the lossless case ($\alpha = 0$),

$$D(\alpha = 0) = 2,$$

which is the directivity of a 2-element array with uniform amplitude distribution. If the second element has infinite loss, which means that it has no contribution to the radiation

$$D(\alpha \to \infty) = 1,$$

which is expected for a single isotropic element.

For a regular rectangular patch antenna designed to operate at 3.5 GHz on 1.5 *mm*-thick air substrate, the directivity calculated using (4.9) with respect to the surface resistance is shown in Fig. 4.3, where the attenuation constant is from (4.3) and the length is $L \approx \lambda/2$. Since the surface resistance of a transparent antenna is achievable to be less than 10 Ω□, the directivity does not significantly reduce in this range.

4.2.3 Radiation Efficiency and Gain Reduction

It has been shown in [31] that a rectangular microstrip antenna can be modeled reasonably well by a dielectric-loaded cavity with two perfectly conducting electric walls and four perfectly conducting magnetic walls. However, it should be noted that this model is a good approximation when the height is very small and the metal has a sufficiently good conductivity.

Assuming that the dominant mode within the cavity is TM_{010}^{x} and considering the patch geometry in Fig. 4.1, the electric and magnetic field components are [31]:

$$\begin{aligned} E_x &= E_0 \cos(\frac{\pi}{L}y) \\ H_z &= H_0 \sin(\frac{\pi}{L}y), \end{aligned} \tag{4.10}$$

where $E_0 = -j\omega A_{010}$ and $H_0 = (\pi/\mu L)A_{010}$.

According to the equivalent current densities, this model also states that there are two radiating slots which account for most of the radiation. The far-zone electric fields radiated by one slot are

$$\begin{aligned} E_r = E_\theta &= 0 \\ E_\phi &= j\frac{k_0 h W E_0 e^{-jk_0 r}}{2\pi r}(\sin\theta \frac{\sin X}{X}\frac{\sin Z}{Z}), \end{aligned} \tag{4.11}$$

where

$$\begin{aligned} X &= \frac{k_0 h}{2}\sin\theta\cos\phi \\ Z &= \frac{k_0 W}{2}\cos\theta. \end{aligned} \tag{4.12}$$

Ideally, the two radiating slots are separated by a very low-impedance parallel-plate transmission line of an effective length L_e and they are of the same magnitude and phase. However, it is suspected that one of the slots has a reduced magnitude due to the conductor loss in the transmission line. Accordingly, the array factor for the two radiating slots is arranged as

$$AF = 1 + e^{-\alpha L} e^{jk_0 L_e \sin\theta \sin\phi}, \tag{4.13}$$

Then, the total far-zone electric fields radiated by the antenna become

$$E_{\phi}^{t} = j\frac{k_0 hW E_0 e^{-jk_0 r}}{2\pi r}(\sin\theta\frac{\sin X}{X}\frac{\sin Z}{Z})(AF). \tag{4.14}$$

The total radiated power is

$$\begin{aligned} P_{rad} &= \frac{1}{2\eta_0}\iint_S |E_{\phi}^{t}|^2 ds \\ &= \frac{2|E_0|^2}{\eta_0 \pi^2 k_0^2} I, \end{aligned} \tag{4.15}$$

where the integral is

$$I = \int_{-\pi/2}^{\pi/2}\int_{0}^{\pi} |\frac{\sin(\frac{k_0 h}{2}\sin\theta\cos\phi)}{\sin\theta\cos\phi}\frac{\sin(\frac{k_0 W}{2}\cos\theta)}{\cos\theta}|^2 |AF|^2 \sin^3\theta d\theta d\phi. \tag{4.16}$$

Here, it should be noted that $|AF|$ is not significantly effective inferred from the directivity analysis.

When the patch conductor is very thin (smaller than the skin depth), some power is lost on the surface, which leads to a significant reduction in the radiation efficiency. To determine the reduction, the antenna geometry shown in Fig. 4.4, is investigated.

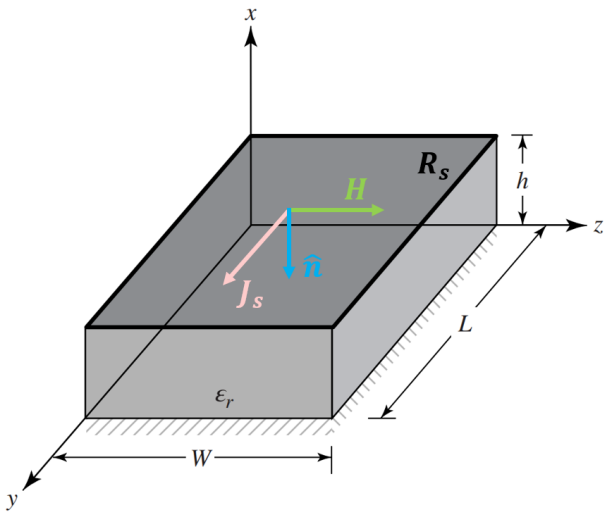

Figure 4.4: Antenna geometry and the surface current vector on the patch.

Power lost on the patch P_{loss} is

$$P_{loss} = \frac{1}{2}\int R_s |\mathbf{J}_s|^2 ds, \tag{4.17}$$

where $\mathbf{J}_s$ is the surface current density and defined as

$$\mathbf{J}_s = \hat{\mathbf{n}} \times \mathbf{H} = \hat{\mathbf{a}}_y H_0 \sin\left(\frac{\pi}{L} y\right) \tag{4.18}$$

using magnetic field intensity vector $\mathbf{H}$ for the dominant mode TM^x_{010} in the cavity as found in [31].

Then, the power loss can be calculated as

$$\begin{aligned} P_{loss} &= \frac{R_s |H_0|^2}{2} \int_0^W \int_0^L |\sin\left(\frac{\pi}{L} y'\right)|^2 dy' dz' \\ &= \frac{1}{4} R_s |H_0|^2 W L \\ &= \frac{\pi^2 R_s}{4\omega^2 \mu^2} \frac{W}{L} |E_0|^2 \\ &= \frac{\pi^2 R_s}{4k^2 \eta^2} \frac{W}{L} |E_0|^2. \end{aligned} \tag{4.19}$$

Using the radiated power (4.15) and the power loss (4.19), radiation efficiency of the antenna can be calculated as

$$e_r = \frac{P_{rad}}{P_{rad} + P_{loss}} \tag{4.20}$$

$$= \frac{\frac{2|E_0|^2}{\eta_0 \pi^2 k_0^2} I}{\frac{2|E_0|^2}{\eta_0 \pi^2 k_0^2} I + \frac{\pi^2 R_s}{4k^2 \eta^2} \frac{W}{L} |E_0|^2}$$

$$= \frac{1}{1 + \frac{\pi^4}{8\eta_0 \mu_r^2} \frac{W}{L} \frac{R_s}{I}}. \tag{4.21}$$

To have a better view in the radiation efficiency in terms of the design parameters, I can be evaluated in the boresight direction ($\theta = \pi/2$). Then, it is found that the integral I depends on the operational frequency f, the substrate height h and the surface resistance R_s. As f and h increase, I also increases, which improves the efficiency. On the other hand, as R_s gets larger, I reduces and R_s/I increases, which in turn yields a worse efficiency as expected.

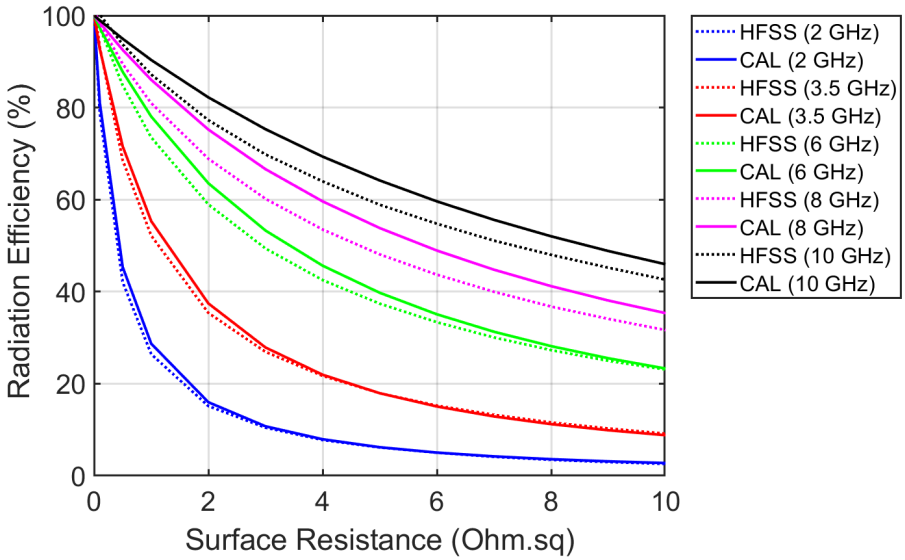

Figure 4.5: Radiation efficiency vs R_s for the patch antennas on 1.5 *mm*-thick air substrate at different frequencies.

To validate the radiation efficiency derivation, several rectangular patch antennas have been designed using the design guidelines (formulas for W and L) in [31] at different frequencies. The antennas have been simulated in HFSS to find radiation efficiency for a range of R_s between 0.01 and 10 $\Omega\square$. For the same configuration, the efficiencies are also calculated in MATLAB using 4.21. Fig. 4.5 shows the simulated and calculated efficiencies of the patch antennas (1.5 *mm*-thick air substrate) at several frequencies. The results are quite consistent at 2 GHz and 3.5 GHz. As the frequency increases, calculated efficiency deviates from the simulated one. Fig. 4.6 shows the efficiencies of two patch antennas with 0.5 *mm*- and 1.5 *mm*-thick air substrates at 10 GHz. For the thinner substrate, the efficiency estimation is nearly the same as the simulation result. When the substrate height is increased, the physical length (L) of the radiating patch decreases relatively. The fringing fields increase, and the antenna becomes a more effective radiator, which in turn increases the radiation efficiency.

In conclusion, the analytical derivation yields reasonably good results for the radiation efficiency of a lossy rectangular patch antenna having a sufficiently thin dielectric substrate in terms of height-to-width ratio or wavelengths. When the substrate is relatively thicker, the cavity model fields used in the derivation might become insufficient to represent the actual fields required for the correct efficiency.

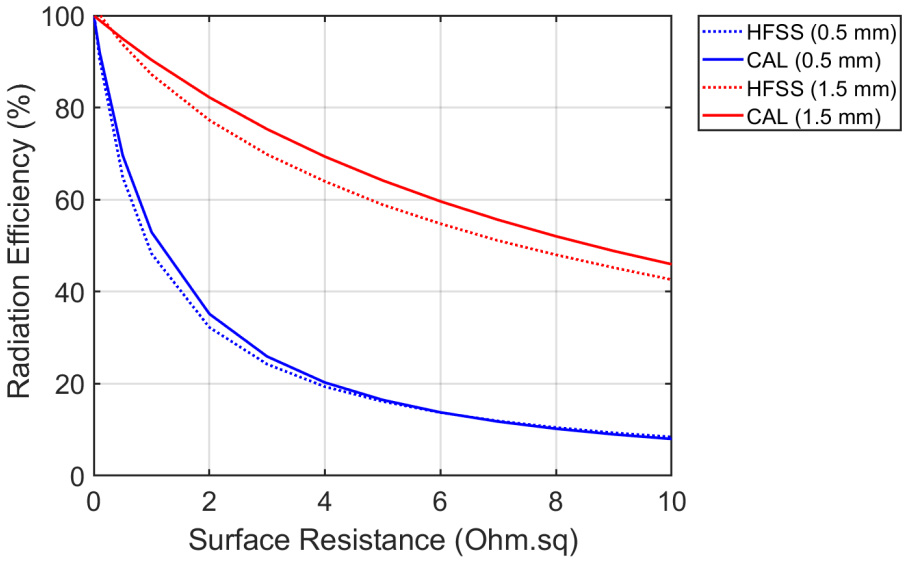

Figure 4.6: Radiation efficiency at 10 GHz vs R_s for the patch antennas on 0.5 *mm*-thick (*L*=14.3 *mm*) and 1.5 *mm*-thick (*L*=12.9 *mm*) air substrates.

4.3 Methods for Gain Enhancement

In this section, methods to improve the gain of transparent patch antennas are proposed by considering the analysis of loss factors, which are summarized as follows:

- For a transparent conductive patch antenna, whose radiating patch has a surface resistance less than or in the vicinity of 10 Ω□, the directivity does not change significantly.

- The major contribution to the gain reduction comes from the conductor loss. Accordingly, a transparent conductor with a low surface resistance and a higher optical transparency is always preferred.

- The antenna radiates more efficiently at a higher operational frequency.

- A thicker substrate or spacer leads to a higher efficiency as long as it is kept within the range of radiating patch antenna conditions and where the surface waves are not significant.

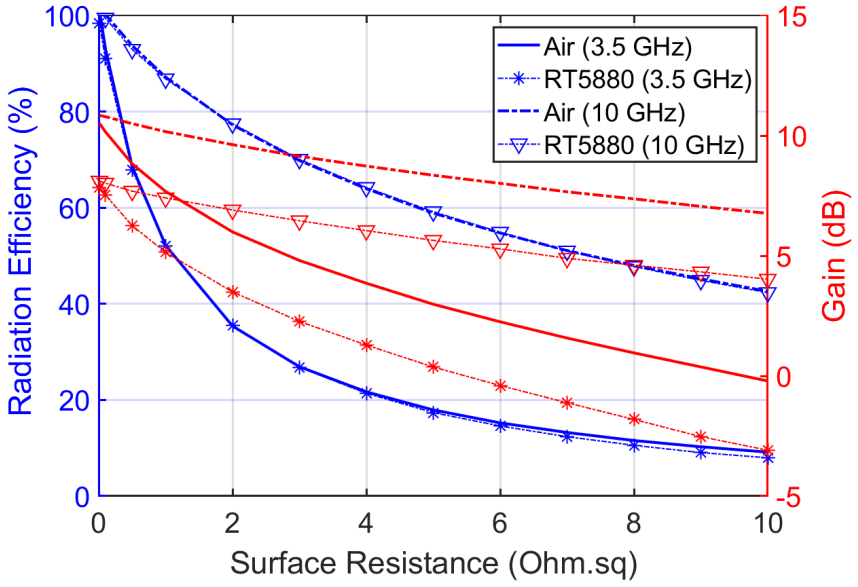

Figure 4.7: Radiation efficiency and gain with respect to surface resistance for a rectangular patch antenna on air slab and on RT5880 with the same thickness $h = 1.5\ mm$ (Ground plane is PEC).

4.3.1 Operational Frequency and Choice of Material

The radiation efficiency analysis indicates that an increase in frequency and substrate height results in a significant loss reduction. Accordingly, HFSS studies were set up for verification. Several patch antennas, whose patches are assigned to surface resistance from 0 to 10 Ω□ and ground planes are PEC, are designed on 1.5 *mm*-thick air spacer and 1.5 *mm*-thick RT5880 at 3.5 GHz and 10 GHz. The results are summarized in Fig. 4.7 and Table 4.1. Fig. 4.7 shows that the efficiency of a patch antenna is improved by choosing a conductor with low R_s (limited by the material science [28]), and by operating at a higher frequency. Besides, it is seen that the antennas on air and RT5880 have the same radiation efficiency at the same frequency. Since a substrate with lower ϵ gives a higher directivity, an air substrate may be the most desirable choice to have a higher gain. Table 4.1 verifies the gain and radiation efficiency improvement with a thicker substrate. It should be noted that when a dielectric is used instead of air, then h is bounded by the rise of surface wave [34].

Table 4.1: Transparent Patch Antenna on Air Slab at 10 GHz

h	Directivity	Gain	Efficiency
1.5 mm	10.5 dBi	6.76 dBi	42.6%
1.0 mm	10.5 dBi	4.63 dBi	26.9%
0.8 mm	10.5 dBi	3.20 dBi	19.6%

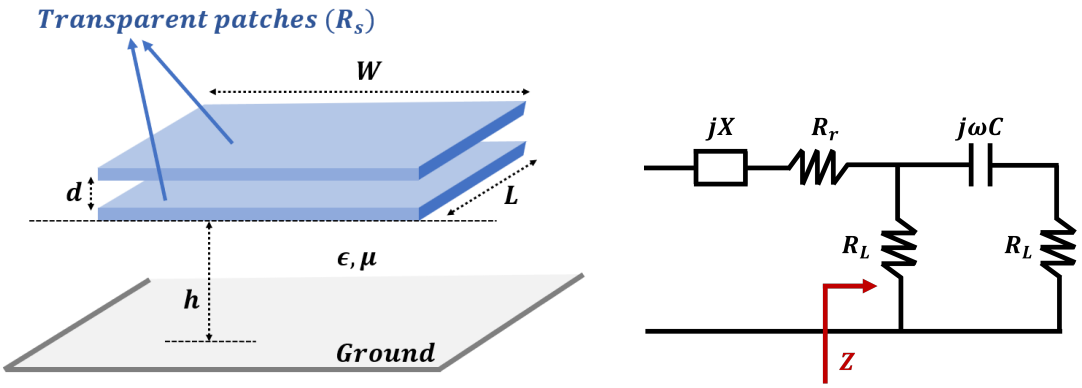

(a) (b)

Figure 4.8: (a) Closely layered patch geometry and (b) its impedance model.

4.3.2 Close Layering of Conductive Films

It is known that the surface resistance of a thin transparent conductive film is subject to material preparation. For higher optical transparency, a thinner film is needed, which leads to a higher R_s. A typical R_s for an 80% transparent AgNW film of 200 *nm*-thick is about 10 $\Omega\square$. Attempts to reduce R_s to half by increasing the AgNW thickness lead to a darker film where the optical transmittance is less than 60%. In addition, a thicker AgNW film might face some structural problems, such as cracks. Alternatively, coating both sides of a PET film with thin AgNW or closely laying multiple such PET films on top of each other are proposed. In this way, the reduction in the optical transparency is less than the one when the thickness of a single AgNW film is increased.

Two layered thin films (such as PET) coated with AgNW as radiating patches are modeled as in Fig. 4.8. When the bottom patch is excited with a probe, it couples to

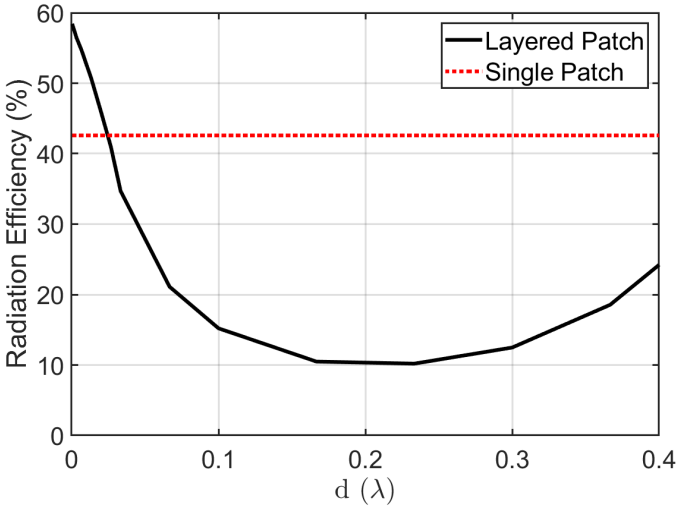

Figure 4.9: Radiation efficiency with respect to layering distance d for a layered patch antenna on air slab with the thickness $h = 1.5\ mm$ at 10 GHz (Ground plane is PEC).

the film above it, making it into a radiating element as well. The loss resistance in the circuit model of close layering as shown in Fig. 4.8b is

$$\begin{aligned} Re\{Z\} &= R_{\text{loss}} \\ &= Re\left\{R_L \parallel \left(R_L + \frac{1}{j\omega C}\right)\right\}, \end{aligned} \tag{4.22}$$

where R_{loss} is the total loss resistance, R_L is the loss resistance due to a single AgNW layer and C is the capacitance between the layers. Since the layers are placed very close, the array factor is nearly 1 and therefore the total radiation resistance R_r remains the same. The loss resistance, however, is affected by the capacitive coupling C. When the films are close as $d = 0$ (Fig. 4.8a), the total loss resistance is reduced to half of the loss resistance of one patch antenna, $R_L/2$. Therefore, it yields an improved antenna efficiency. To observe the effect of the distance (d) between the layers, a second AgNW layer is added to the single layer patch antenna on 1.5 *mm*-thick air slab with PEC ground. This layered patch antenna is simulated for various d at 10 GHz. The efficiency results are given in Fig. 4.9. It follows a similar curve estimated by (4.22) as d is increased. For the single layer case, the antenna efficiency at 10 GHz is 42.6% as reported in Table 4.1. When $d < 0.025\lambda$, the efficiency for the layered patch is higher than that of the single patch.

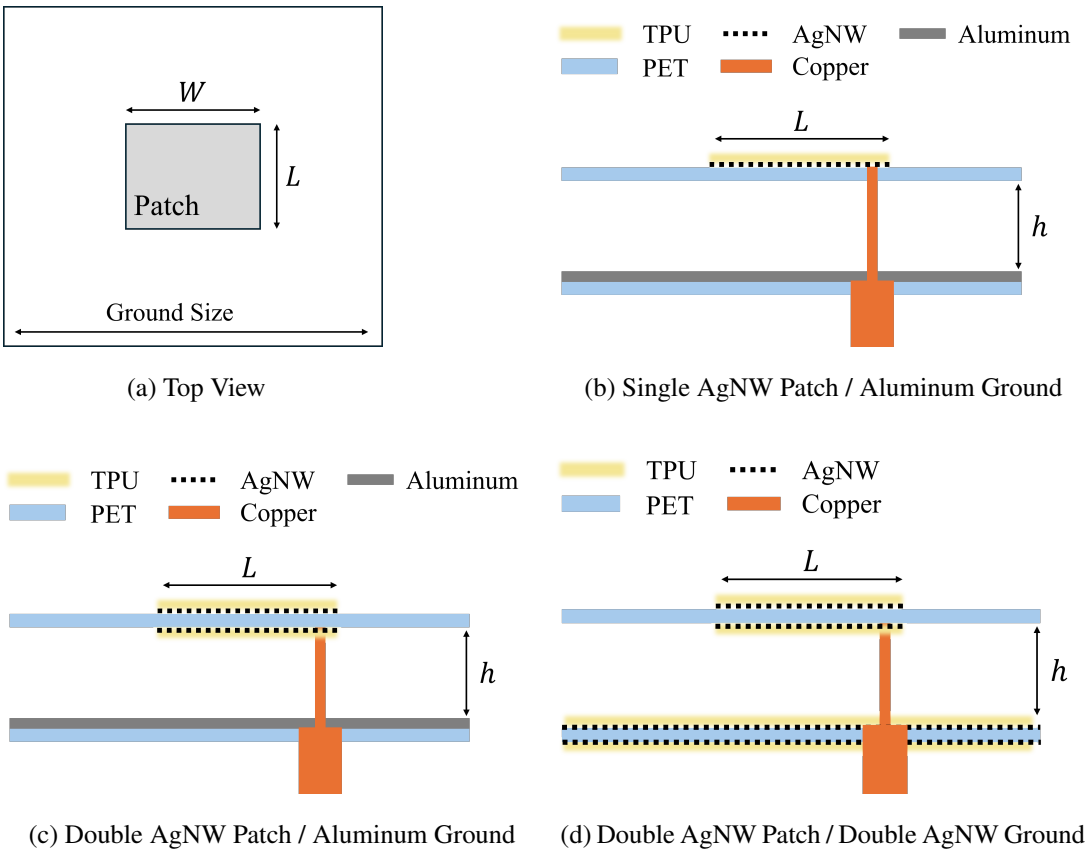

(a) Top View

(b) Single AgNW Patch / Aluminum Ground

(c) Double AgNW Patch / Aluminum Ground

(d) Double AgNW Patch / Double AgNW Ground

Figure 4.10: Transparent patch antenna geometries: top view and side views.

4.4 AgNW Transparent Patch Antennas, Fabrication, and Measurements

Following the analysis of loss factors and gain improvement methods, several patch antenna prototypes, which are fed by coaxial probes, in different configurations are fabricated. The geometries of these AgNW patch antenna configurations are illustrated in Fig. 4.10. In all configurations, antenna dimensions are the same, where $L = 13\ mm$, $W = 14\ mm$, Ground Size$= 50\ mm$, and the air substrate thickness $h = 1.5\ mm$.

AgNW samples are prepared as described in Ch. 2. Examples of the samples including single-sided and double-sided patches, and double-sided patch antenna assemblies, are as shown in Fig. 4.11. The single-sided patch sample is created by coating one side of a PET film (127 μm-thick) with AgNWs and protecting it with a TPU (approximately 127 μm-thick) protection layer. On the other hand, the double-sided

(a) (b) (c)

Figure 4.11: AgNW patch antenna samples: (a) Single-sided sample, (b) double-sided sample, and (c) double-sided patch antenna assembly.

patch involves coating both sides of the PET film with AgNWs, with TPU covering all areas exposed to air for protection. This design implements the closely layered transparent conductor approach proposed in the previous section. The transparent patch antenna is then assembled using a plastic frame to maintain a 1.5 *mm*-thick air spacer between the patch and the ground plane. Connections to the SMA connector are established using low-temperature silver paste. For comparison, a reference antenna is also constructed by replacing the AgNW-coated layers with aluminum tape pasted to the PET film, following the same assembly process and using the same frame and SMA connector.

The three patch antenna configurations from single-sided or double-sided AgNW samples and the reference antenna fully made of aluminum are measured with vector network analyzer. Measured S parameter results are given in Fig. 4.12 together with the simulation results performed in HFSS. Even though the analyses in the previous sections focus on 10 GHz, it is seen that the resonances of the prototypes are shifted to around 8.9 GHz. This is expected because the multiple PET and TPU films extend the effective length of the patch by increasing the effective dielectric constant compared to air. Slight differences between the resonance frequencies of simulation and measurement data might be due to the misalignment of the pin locations during prototype assembly. Besides, all S_{11} results exhibits losses in out-of-band regions compared to the simulations. This is likely caused by the pin connections to the patch and the

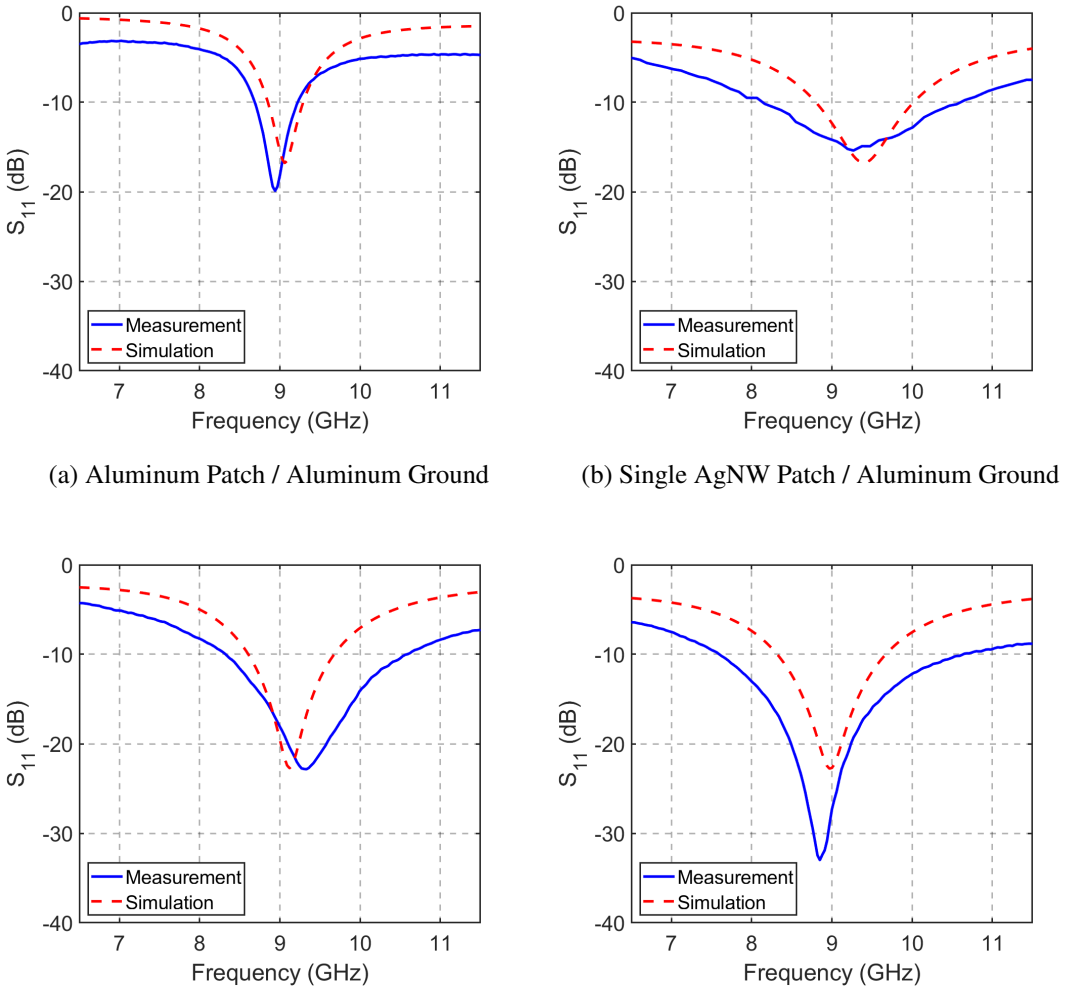

(a) Aluminum Patch / Aluminum Ground

(b) Single AgNW Patch / Aluminum Ground

(c) Double AgNW Patch / Aluminum Ground

(d) Double AgNW Patch / Double AgNW Ground

Figure 4.12: Measured and simulated S parameters of four patch antenna prototypes.

ground via the low-temperature silver paste. Nevertheless, all S_{11} measurements are consistent with the simulations, confirming the reliability of the results.

Gain and radiation pattern measurements are performed in the anechoic chamber to evaluate the performance of the antenna prototypes. Table 4.2 presents the measured gain and radiation efficiency (e_T) at 8.9 GHz alongside the simulation results. The aluminum patch with an aluminum ground achieves 7.14 dBi gain and serves as the reference. Using a single-sided AgNW patch with an aluminum ground significantly reduces the gain to 2.81 dBi. When it is replaced by the double-sided AgNW patch with an aluminum ground, the gain increases to 4.31 dBi, while changing both the

Table 4.2: Measured Radiation Efficiency and Gain of Patch Antenna Prototypes at 8.9 GHz

Patch Type	Ground Type	Max. Gain (Simulation)	Max. Gain (Measurement)	Efficiency (e_T) (Simulation)	Efficiency (e_T) (Measurement)
Aluminum	Aluminum	9.94 dBi	**7.14 dBi**	Ref.	**Ref.**
Single AgNW	Aluminum	5.55 dBi	**2.81 dBi**	37.8%	**36.9%**
Double AgNW	Aluminum	7.17 dBi	**4.31 dBi**	54.7%	**52.1%**
Double AgNW	Double AgNW	6.08 dBi	**3.58 dBi**	43.7%	**44.0%**

patch and ground with double-sided AgNW films have the gain of 3.58 dBi. Since making the ground transparent with AgNW further reduces the gain, it should be noted that a single-sided patch with a single-sided ground would result in a gain lower than 2.81 dBi.

A common trend between the measured and simulated gains is evident, with measured gains consistently lower by at least 2.5 dB. This loss is attributed to factors unrelated to transparency or the loss in AgNW, such as connection quality and the use of low-temperature silver adhesive. The efficiency denoted as e_T is the radiation efficiency which is only related to the loss on the AgNW films so the transparency. It is calculated from the measured gain reduction compared to the reference antenna gain. For instance, the double AgNW patch with aluminum ground prototype has a measured gain of 4.31 dBi, which is 2.83 dB less than the reference gain of 7.14 dBi. Thus, e_T is found as 52.1%. Accordingly, the efficiencies (e_T) of the single AgNW patch with aluminum ground and the double AgNW patch with double AgNW ground prototypes are also calculated as 36.9% and 44.0%, respectively.

In simulations, where connection losses and adhesive effects are absent, simulated e_T represents only transparency-related losses caused by the AgNW films. Consequently, simulated and measured e_T values closely align, confirming that the observed efficiency losses are primarily due to the transparency-related properties of the AgNW layers. This consistency between simulation and measurement underscores the reliability of the design and performance evaluation process.

Table 4.3: Optical Transmittance and Efficiencies at 8.9 GHz for Different Transparent Patch Antenna Configurations

Conductive Films	Surface Resistance	AgNW Transparency	Patch Type	Ground Type	Efficiency (e_T) (Simulation)	Efficiency (e_T) (Measurement)
Single AgNW ($200\ nm$)	10 Ω□	80%	Single	Aluminum	37.8%	**36.9%**
			Single	Single	29.5%	-
Thicker Single AgNW ($\sim 350 - 400\ nm$)	~6 Ω□	60%	Single	Aluminum	49.7%	-
			Single	Single	41.0%	-
Double AgNW ($2 \times 200\ nm$)	10 Ω□ For Each	64%	Double	Aluminum	54.7%	**52.1%**
			Double	Double	43.7%	**44.0%**

Considering transparency, Table 4.3 highlights the trade-off between optical transmittance and radiation efficiency (e_T) for various patch antenna configurations using AgNW films. The single 200 *nm* AgNW film achieves the highest optical transmittance (80%), making it the most transparent option, but it results in the lowest radiation efficiencies, with the measured 36.9% efficiency when paired with an aluminum ground and the simulated 29.5% with a single AgNW ground. On the other hand, the thicker single AgNW film (350–400 *nm*) reduces optical transmittance to 60% or even lower, but it improves the efficiency, achieving 49.7% with an aluminum ground and 41.0% with a single AgNW ground. This suggests that increasing the AgNW thickness enhances electromagnetic performance by reducing losses but compromises transparency. However, thickening the AgNW layer to 400 *nm* might lead to structural challenges such as possible cracks.

Instead of increasing the thickness of a single AgNW layer, using two closely layered single AgNW films (200 *nm* each) has been proposed and provides a balanced solution. This configuration achieves a moderate optical transmittance of 64%, while the radiation efficiency reaches 52.1% with an aluminum ground and 44.0% with a double AgNW ground as measured. The layered structure might mitigate the mechanical challenges associated with thicker AgNW films, making it advantageous unless those issues are resolved. This approach maintains a reasonable level of transparency while significantly improving the radiation efficiency compared to a single sided AgNW (200 *nm*) film. It should also be noted that the transparency values given above are for the AgNW films without TPU cover, which might reduce the overall transparency

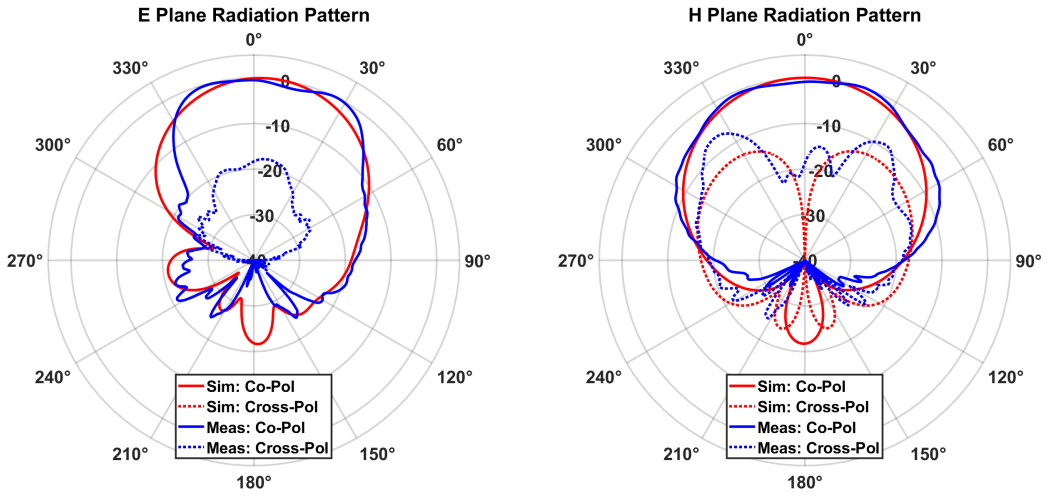

(a) (b)

Figure 4.13: Radiation patterns of proposed transparent patch antenna (double-sided patch + double-sided ground) at 8.9 GHz: (a) E-plane and (b) H-plane.

as well. The transparency of TPU cover might differ with its production cycle. That's why it is kept out of the discussion.

The radiation pattern measurements of the proposed double AgNW patch antenna at 8.9 GHz (Fig. 4.13) show good agreement with the simulation results. The co-polarization (Co-Pol) patterns in both the E-plane and H-plane align well with the simulated results, demonstrating the accuracy of the design and modeling process. The discrepancy in the Cross-Pol patterns between the measured and simulated results can be attributed to non-idealities in the measurement, including potential effects of holders, cables, or other equipment that could introduce undesired reflections.

In conclusion, the proposed double AgNW patch antenna demonstrates a gain of 3.58 dBi and an efficiency of 44% at 8.9 GHz, making it a promising candidate for applications requiring optical transparency and acceptable electromagnetic performance. Its radiation patterns exhibit characteristics expected of a patch antenna, with good agreement between simulations and measurements in the co-polarization component. The antenna effectively balances transparency, electromagnetic performance, and structural concerns related to material science.

CHAPTER 5

CONCLUSION

This thesis explores the analysis, design, and fabrication of optically transparent antennas made of nanowire networks, addressing the critical trade-offs between optical transparency and radiation performance. The research focuses on two primary types of transparent antennas: monopole and patch designs, each with distinct design considerations and performance characteristics.

The transparent monopole antenna is designed for sub-6 GHz 5G and V2X applications. The effects of various geometric parameters, such as length, width, and surface resistance are thoroughly studied using reliable analytical methods. It is shown that these parameters significantly impact radiation efficiency, as inferred from the loss resistance formula, which effectively estimates gain reduction. The antenna's length is primarily associated with the operational frequency, while surface resistance is determined by material preparation. It is demonstrated that improving radiation efficiency can be more effectively achieved by widening the monopole and adding highly conductive strips to regions with densely induced current, rather than modifying material properties or layering transparent conductors. This approach not only enhances efficiency but also results in a wide-band frequency response with minimal impact on optical transparency. Furthermore, methods for reducing cross-polarization levels have been presented. Transparent monopole antenna prototypes are fabricated with spraying of silver nanowires on a flexible substrate, PET. They are fed by CPW line which can be hidden inside the frames of the windows or windshields. It is demonstrated that the fabricated antenna prototypes have optical transparency as high as 80% and efficiencies of 50.4% for the monopole without a solid conductor strip and 76.3% for the one with the bottom strip, which is higher than reported prior art.

A transparent patch antenna is introduced, with both the radiator and ground plane fabricated using AgNW networks applied via airbrushing onto PET substrates. The research explores key factors contributing to reduced radiation efficiency and gain as done for the monopole antenna. Several approaches are proposed, including the use of thicker substrates, operation at higher frequencies, and the introduction of a closely layered structure. This layered design, achieved by coating both sides of the PET substrate with AgNW, is considered with a circuit model and achieves a lower loss resistance when the distance between the two layers are within the limit set by the single layer patch antenna. For validation purposes, prototype configurations include a single-sided AgNW patch antenna, where PET film is coated on one side with AgNWs and protected by TPU; a double-sided AgNW patch antenna, where both sides of the PET are coated with AgNWs and fully covered with TPU; and a reference antenna, fabricated using aluminum tape on PET film. Performance analysis reveals that the aluminum reference patch achieves a gain of 7.14 dBi, while the single-sided AgNW patch attains a gain of 2.81 dBi and an efficiency of 36.9%. The double-sided AgNW patch with an aluminum ground shows improved performance with a gain of 4.31 dBi and an efficiency of 52.1%, whereas the fully AgNW patch and ground structure achieves a gain of 3.58 dBi and an efficiency of 44%. In addition, thinner AgNW layer (200 nm) on aluminum ground provides high transparency (80%) but lower efficiency, whereas the layering approach using two 200 nm AgNW layers achieves a balance of 64% transparency. Radiation patterns exhibit good alignment with simulations, confirming that the double-layered AgNW design offers an effective balance between optical transparency and radiation performance, making it suitable for various applications like smart displays and architectural glass.

In this research, AgNWs were selected as the primary material for fabricating transparent conductive layers due to their ease of deposition and cost-effectiveness compared to other alternatives like ITO. While ITO has been extensively studied for its transparent conductive properties, fabrication of such materials often involves complex processes such as magnetron sputtering, photolithography, and clean-room operations, which increase production costs and complexity. In contrast, AgNWs can be deposited using simple techniques like airbrushing, making them more practical for prototyping.

The broader implications of this research are significant, contributing to the advancement of technologies in areas such as V2X communication, smart buildings, wearable devices, and transparent displays for 5G and beyond. The methodologies and findings presented in this thesis pave the way for further innovations in optically transparent antenna designs.

Future research directions could include exploring the performance of the designed AgNW antennas when applied to windows, windshields, or other transparent surfaces specific to chosen applications. The positioning of these antennas and their feeding structures can be studied and optimized for the best functionality. For example, a study on positioning could investigate how the radiation pattern is affected and determine the optimal placement on various transparent surfaces. Additionally, the feeding structures, such as connectors, pose another challenge. A mechanically flexible monopole antenna, for instance, may require more suitable connectors for integration into the application. In this research, the use of low-temperature silver adhesive for connecting the feed to the antenna leads to significant losses, which might be undesirable. Therefore, exploring better adhesives or alternative methods for feed connection could be an important aspect of future work.

In conclusion, this thesis presents a foundation for the development of optically transparent monopole and patch antennas made of AgNw networks, addressing both theoretical challenges and practical implementation.

REFERENCES

[1] M. N. Abbasi, A. Aziz, K. A. Aljaloud, A. R. Chishti, Y. T. Aladadi, and R. Hussain, "A close proximity 2-element MIMO antenna using optically transparent wired-metal mesh and polyethylene terephthalate material," *IEEE Access*, vol. 11, pp. 78811–78819, 2023.

[2] Z. J. Silva, C. R. Valenta, and G. D. Durgin, "Optically transparent antennas: A survey of transparent microwave conductor performance and applications," *IEEE Antennas and Propagation Magazine*, vol. 63, no. 1, pp. 27–39, 2021.

[3] R. B. Green, M. Guzman, N. Izyumskaya, B. Ullah, S. Hia, J. Pitchford, R. Timsina, V. Avrutin, U. Ozgur, H. Morkoc, N. Dhar, and E. Topsakal, "Optically transparent antennas and filters: A smart city concept to alleviate infrastructure and network capacity challenges," *IEEE Antennas and Propagation Magazine*, vol. 61, no. 3, pp. 37–47, 2019.

[4] G. Clasen and R. Langley, "Meshed patch antennas," *IEEE Transactions on Antennas and Propagation*, vol. 52, no. 6, pp. 1412–1416, 2004.

[5] K. An, P. Sun, Y. Deng, and A. Chen, "A large-scale high-gain transparent grid array antenna for millimeter-wave communication," *IEEE Antennas and Wireless Propagation Letters*, vol. 23, no. 5, pp. 1598–1602, 2024.

[6] Y. Morimoto, S. Shiu, I. W. Huang, E. Fest, G. Ye, and J. Zhu, "Optically transparent antenna for smart glasses," *IEEE Open Journal of Antennas and Propagation*, vol. 4, pp. 159–167, 2023.

[7] H.-T. Hu, B.-J. Chen, and C. H. Chan, "A transparent proximity-coupled-fed patch antenna with enhanced bandwidth and filtering response," *IEEE Access*, vol. 9, pp. 32774–32780, 2021.

[8] J. Park, S. Y. Lee, J. Kim, D. Park, W. Choi, and W. Hong, "An optically invisible antenna-on-display concept for millimeter-wave 5G cellular devices,"

IEEE Transactions on Antennas and Propagation, vol. 67, no. 5, pp. 2942–2952, 2019.

[9] T. Yasin and R. Baktur, "Bandwidth enhancement of meshed patch antennas through proximity coupling," *IEEE Antennas and Wireless Propagation Letters*, vol. 16, pp. 2501–2504, 2017.

[10] X. W. Dai, Y. H. Zhang, Z. Li, W. Yu, L. Liu, and G. Q. Luo, "Optically transparent circularly polarized reflectarray for Ka-band applications," *IEEE Transactions on Antennas and Propagation*, vol. 72, no. 6, pp. 5414–5419, 2024.

[11] H. Chang, F.-P. Lai, and Y.-S. Chen, "Transparent transmitarray antenna with large aperture for significant gain enhancement in millimeter-wave 5G communication networks," *IEEE Antennas and Wireless Propagation Letters*, vol. 23, no. 2, pp. 663–667, 2024.

[12] A. S. M. Sayem, D. Le, R. B. V. B. Simorangkir, T. Björninen, K. P. Esselle, R. M. Hashmi, and M. Zhadobov, "Optically transparent flexible robust circularly polarized antenna for UHF RFID tags," *IEEE Antennas and Wireless Propagation Letters*, vol. 19, no. 12, pp. 2334–2338, 2020.

[13] D. Potti, Y. Tusharika, M. G. N. Alsath, S. Kirubaveni, M. Kanagasabai, R. Sankararajan, S. Narendhiran, and P. B. Bhargav, "A novel optically transparent UWB antenna for automotive MIMO communications," *IEEE Transactions on Antennas and Propagation*, vol. 69, no. 7, pp. 3821–3828, 2021.

[14] K. K. So, B.-J. Chen, and C. H. Chan, "Microwave and millimeter-wave MIMO antenna using conductive ITO film," *IEEE Access*, vol. 8, pp. 207024–207033, 2020.

[15] S. Hong, S. H. Kang, Y. Kim, and C. W. Jung, "Transparent and flexible antenna for wearable glasses applications," *IEEE Transactions on Antennas and Propagation*, vol. 64, no. 7, pp. 2797–2804, 2016.

[16] C. Kocia and S. V. Hum, "Design of an optically transparent reflectarray for solar applications using indium tin oxide," *IEEE Transactions on Antennas and Propagation*, vol. 64, no. 7, pp. 2884–2893, 2016.

[17] J.-W. Kim, J.-I. Oh, K.-S. Kim, J.-W. Yu, K.-J. Jung, and I.-N. Cho, "Efficiency-improved UWB transparent antennas using ITO/Ag/ITO multilayer electrode films," *IEEE Access*, vol. 9, pp. 165385–165393, 2021.

[18] R. B. Green, K. Ding, V. Avrutin, U. Ozgur, and E. Topsakal, "Optically transparent antenna arrays for the next generation of mobile networks," *IEEE Open Journal of Antennas and Propagation*, vol. 3, pp. 538–548, 2022.

[19] Y. Goliya, A. Rivadeneyra, J. F. Salmeron, A. Albrecht, J. Mock, M. Haider, J. Russer, B. Cruz, P. Eschlwech, E. Biebl, M. Becherer, and M. R. Bobinger, "Next generation antennas based on screen-printed and transparent silver nanowire films," *Advanced Optical Materials*, vol. 7, no. 21, p. 1900995, 2019.

[20] Q. H. Dao, R. Tchuigoua, B. Geck, D. Manteuffel, P. von Witzendorff, and L. Overmeyer, "Optically transparent patch antennas based on silver nanowires for mm-wave applications," in *2017 IEEE International Symposium on Antennas and Propagation & USNC/URSI National Radio Science Meeting*, pp. 2189–2190, 2017.

[21] T. W. Turpin and R. Baktur, "Meshed patch antennas integrated on solar cells," *IEEE Antennas and Wireless Propagation Letters*, vol. 8, pp. 693–696, 2009.

[22] M. S.-S. Shahin Sheikh and M.-M. Bagheri-Mohagheghi, "Transparent microstrip antenna made of fluorine doped tin oxide: a comprehensive study," *Journal of Electromagnetic Waves and Applications*, vol. 29, no. 12, pp. 1557–1569, 2015.

[23] P. Drude, "Zur Elektronentheorie der Metalle; II. Teil. Galvanomagnetische und thermomagnetische Effecte," *Annalen der Physik*, vol. 308, pp. 369–402, Jan. 1900.

[24] H. Askari, H. Fallah, M. Askari, and M. C. Mohmmadieyh, "Electrical and optical properties of ITO thin films prepared by dc magnetron sputtering for low-emitting coatings," *arXiv preprint arXiv:1409.5293*, 2014.

[25] M. E. Eralp, O. Cakir, O. Aydin Civi, H. E. Unalan, and R. Baktur, "Transparent conductive nanowire antennas-material preparation, characterization, and notes on antenna design," in *2024 IEEE International Symposium on Antennas and*

Propagation and INC/USNC-URSI Radio Science Meeting (AP-S/INC-USNC-URSI), pp. 2701–2702, 2024.

[26] M. E. Eralp, O. Aydin Civi, and R. Baktur, "Highly transparent and efficient flexible antenna for vehicle-to-everything (V2X) applications," in *2024 18th European Conference on Antennas and Propagation (EuCAP)*, pp. 01–04, 2024.

[27] M. E. Eralp, R. Baktur, and O. Aydin Civi, "Analysis and improvement on the gain of optically clear silver nanowire patch antenna," in *2024 IEEE International Symposium on Antennas and Propagation and INC/USNC-URSI Radio Science Meeting (AP-S/INC-USNC-URSI)*, pp. 2687–2688, 2024.

[28] T. Yasin, R. Baktur, and C. Furse, "A study on the efficiency of transparent patch antennas designed from conductive oxide films," in *2011 IEEE International Symposium on Antennas and Propagation (APS)*, pp. 3085–3087, 2011.

[29] D. Doganay, O. Demircioglu, M. Cugunlular, M. O. Cicek, O. Cakir, H. U. Kayaci, S. Çınar Aygün, and H. E. Unalan, "Wet spun core-shell fibers for wearable triboelectric nanogenerators," *Nano Energy*, vol. 116, p. 108823, 2023.

[30] O. Cetin, O. Cakir, S. Koylan, D. Doganay, Y. Khan, and H. E. Unalan, "All-solution processed, highly stable MXene/Cu nanowire networks for flexible transparent thin-film heaters," *ACS Applied Nano Materials*, vol. 6, no. 23, pp. 22446–22458, 2023.

[31] C. Balanis, *Antenna Theory: Analysis and Design*. Wiley, 2015.

[32] R. Baktur, M. E. Eralp, and O. Aydin Civi, "Ultra wide band (UWB) character of wide planar monopoles and their potential applications in transparent antenna designs," in *2024 IEEE International Symposium on Antennas and Propagation and INC/USNC-URSI Radio Science Meeting (AP-S/INC-USNC-URSI)*, pp. 1189–1190, 2024.

[33] H. J. Song, T. Y. Hsu, D. F. Sievenpiper, H. P. Hsu, J. Schaffner, and E. Yasan, "A method for improving the efficiency of transparent film antennas," *IEEE Antennas and Wireless Propagation Letters*, vol. 7, pp. 753–756, 2008.

[34] D. Pozar, "Considerations for millimeter wave printed antennas," *IEEE Transactions on Antennas and Propagation*, vol. 31, no. 5, pp. 740–747, 1983.